Mineralogical Magazine, June 2010, Vol. 74(3), pp. 529–551

Feldspars defined and described: a pair of posters published by the Mineralogical Society. Sources and supporting information

I. PARSONS*

Grant Institute of Earth Science, University of Edinburgh, West Mains Road, Edinburgh EH9 3JW, UK

[*Received 28 November 2009; Accepted 7 June 2010*]

ABSTRACT

The Mineralogical Society of Great Britain & Ireland has published two full-colour posters describing the feldspar minerals, designed primarily for student use. They may be downloaded free of charge by all from www.minersoc.org/pages/education/edu.html and are designed to be printed at A3 size, although they are legible at A4 and in greyscale. Sheet 1 deals with nomenclature, crystal structure and phase relationships, while Sheet 2 covers phase behaviour. For brevity no sources are given on the posters, and these are provided in the present article, together with supporting notes and suggested reading on the more complex topics.

Introduction

THE Mineralogical Society has recently produced two A3-sized full-colour poster-style sheets on the feldspar minerals (called Sheet 1 and 2 below), designed for student use. They may be downloaded from www.minersoc.org/pages/education/edu.html. The posters shown in these notes are for illustration only. The versions available on the web are of much higher quality. They are based on the work of mineralogists over nearly a century but for brevity no sources were included and they are provided here. The notes explain the choices made in the content of the sheets, and give more background on a variety of topics. References include papers fundamental for understanding feldspars, concentrating on aspects which are of importance to petrologists and geochemists. Phase diagrams, some of which are composites from several sources, are drawn accurately. Details of physical and optical properties are widely treated in mineralogy textbooks, but many of the most informative features of feldspars are below the resolution of the petrographic microscope and electron microscope images are provided to emphasize the importance of these techniques. Twinning is described to illustrate its value as a guide to crystal orientation, character of phase transitions, and thermal history.

The numbered sections below correspond with superscripted numbers on the posters. The abbreviations Ab, Or and An refer to the $NAlSi_3O_8$, $KAlSi_3O_8$ and $CaAl_2Si_2O_8$ *components*, respectively. PL and AF refer to plagioclase and alkali feldspar *phases* as defined in Sheet 1, Sec. 2 and Fig. 1.2. In general each phase is a *ternary solid solution*. The word 'orthoclase' will be used only for an Or-rich AF with particular structural and optical properties as defined in the caption to Fig. 1.3 and in Note 3. Other acronyms are: XP: crossed polarizers; TEM: transmission electron microscopy; SEM: scanning electron microscopy; SE: secondary electron imaging; BSE: back-scattered electron imaging; XRD: X-ray diffraction.

Specialized sources

There are several books devoted entirely to the feldspar minerals. The most comprehensive are Deer *et al*. (2001), Smith and Brown (1988) and Smith (1974*a,b*). A series of volumes which followed NATO Advanced Study Institutes on feldspars (Christie, 1962; MacKenzie and Zussman, 1974; Brown, 1984; Parsons, 1994)

* E-mail: ian.parsons@ed.ac.uk
DOI: 10.1180/minmag.2010.074.3.529

FELDSPARS 1
Nomenclature, Structure and Phase Relationships

1.1 Introduction. Feldspars are the most abundant mineral species in both the oceanic and continental crust, making up 50–60% by volume. They are framework aluminosilicate minerals with the general formula MT_4O_8, where M is usually Ca^{2+}, Na^{1+} or K^{1+}, and T is Al^{3+} or Si^{4+}, with Al ≥1 and ≤2. They have either monoclinic or triclinic symmetry and exhibit considerable solid solution at high *T*, but very little at low *T*, when almost all natural feldspars are intergrowths of two or more feldspar phases.

Fig 1.1 Polished surface of porphyritic granite from Shap, Cumbria

Feldspars are often pink (like the orthoclase phenocrysts in the granite, **Fig. 1.1**) or white (the plagioclase in the matrix) and variably transparent[1]. This turbidity is caused by large numbers of sub-μm pores produced by reactions with fluids. Crystals that have escaped such reactions are glass clear and colourless in small fragments or dark green in massive samples of plutonic rocks. Most have two prominent cleavages, (010) and (001), at right angles, although these may be poorly developed in volcanic rocks. Triclinic crystals are usually macroscopically monoclinic, because of repeated fine scale twinning[2].

1.2 Components and phases[3]: Common feldspars are ternary solid solutions of three components:

$CaAl_2Si_2O_8$ (anorthite: An)
$NaAlSi_3O_8$ (albite: Ab)
$KAlSi_3O_8$ (orthoclase: Or)

Solid solutions with a predominance of An+Ab form the plagioclase feldspar series, those predominantly composed of Ab+Or form the alkali feldspar series. At stable equilibrium a rock can contain only two feldspar phases, a plagioclase phase (abbreviated here to **Pl**) and an alkali feldspar phase (**Af**).

At room *T* all Pl are triclinic, but in Af only feldspars from Ab_{100} to $Ab_{60}Or_{40}$ are invariably triclinic. At high *T* all Af are monoclinic. There are two mechanisms for the symmetry change. In Af with >Ab_{60} it occurs by a rapid shearing phase transformation caused by twisting of Si- and Al-tetrahedra (ST on **Figs 1.5, 1.7**). In Or-rich Af it takes place by a slow 'diffusive' order-disorder transformation in which Al ions, distributed randomly between four equivalent sites at high *T*, become ordered on one of these sites during cooling (**Fig. 1.4**).

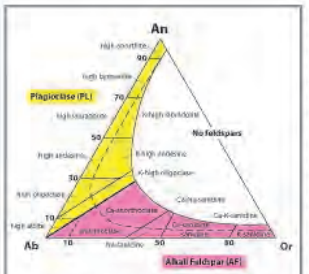

Nomenclature Fig 1.2[4] The maximum extent of solid solution in feldspars, at >1000°C. No feldspars crystallize in the unshaded field. The boundary between plagioclase and alkali feldspar is placed, for convenience only, on the line where An = Or. The named subdivisions of Pl, at 10, 30, 50, 70 and 90% An are based solely on composition. Anorthoclase and high albite are triclinic at room *T* but become monoclinic when observed at elevated *T* because of the shearing transformation. Sanidine is monoclinic at all *T*.

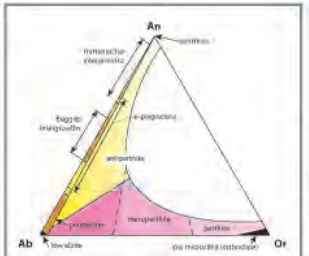

Fig 1.3[5] Feldspars stable below ~300 °C. Solid solution is limited to the black shaded areas. The stable phases are triclinic low microcline, low albite and anorthite, all with Si-Al order. Orthoclase is a metastable monoclinic Or-rich feldspar with a 'tweed' microstructure composed of alternating triclinic ordered domains at the scale of a few nm. In Pl, ordering (giving low plagioclase), leads to changes of lattice type and optical properties but not crystal class (**Fig 1.7**). Pl in the range ~An_{25}–An_{75} has a structure known as *e*-plagioclase in which thin slabs with albite-like and anorthite-like ordering patterns alternate with a periodicity that is out of step ('incommensurate'), with the overall lattice.

1.3 Intergrowths of an Or-rich phase and an Ab-rich phase, known as perthitic intergrowths (**Fig 1.3**), form by exsolution during cooling of homogeneous Af. They are called cryptoperthite when sub-optical, microperthite when visible in an petrographic microscope and macroperthite when visible unaided. The term perthite is used strictly for crystals with an Or-rich bulk composition in which Ab-rich lamellae occur in an Or-rich matrix. Antiperthite has an Ab-rich matrix and mesoperthite has approximately equal proportions of the Ab- and Or-rich phases. Terms such as cryptoantiperthite and micromesoperthite are also used. Cryptomesoperthites can act as diffraction gratings, producing iridescence, seen in the familiar architectural syenite, larvikite.

Low Pl in the fully shaded area near the Ab-An join (**Fig 1.3**), are strongly non-ideal and there are three miscibility gaps leading to sub-optical intergrowths.: Peristerite: An_{2}–An_{15}; Bøggild: An_{35}–An_{52}; Huttenlocher: An_{54}–An_{90}. These sometimes cause optical iridescence. 'Labradorescence' is caused by Bøggild intergrowths. TEM must be used to image these intergrowths.

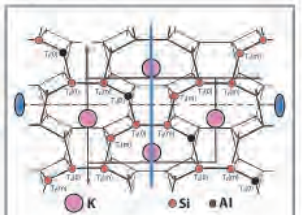

Fig 1.4[5] Structure of sanidine (monoclinic, C2/m) viewed on (001). The framework of T sites is shown, but not the tetrahedra of oxygen surrounding them. The distribution of Si or Al for an ordered feldspar is shown in two diagonal chains, illustrating how symmetry is lost when ordering occurs. Atoms are not to scale.

1.4 Crystal structure and symmetry[3] All feldspar structures are based on **Fig 1.4**. In triclinic feldspars the unit cell is distorted in a right- or left-handed sense relative to the mirror plane ***m*** and the symmetry is lost. The maximum departure of the cell angles from 90° is α 94.3° and γ 87.7° in low albite.

The framework is strong but tetrahedra can tilt in complex ways making it slightly elastic. The M ions occupy large and irregular sites. In AF the M ions have different ionic radii ([8]K^{1+} 0.151, [7]Na^{1+} 0.112 nm) but the same charge, whereas in Pl they have similar radii ([8]Ca^{2+} 0.112 nm) but different charges. For charge balance in Pl, substitution of Ca^{2+} and Al^{3+} must be coupled, leading to fine-scale exsolution microtextures. In AF K and Na can diffuse relatively rapidly through the structure during perthitic exsolution because they are not charge-coupled to the elastic framework.

The framework deforms spontaneously around the M site at the shearing transformation (ST) in Na- and Ca-rich feldspars so that anorthoclase and all Pl are triclinic at room *T*. The ordering transformation[5] is comparatively slow because Al- and Si-O bonds must break in the strong framework. In disordered feldspars, sites labelled T_1 and T_2 in **Fig. 1.4** are occupied at random by Al and Si, but in ordered feldspars Al is located in site $T_1(0)$ (one set is shown as black circles) and symmetry is lost. There are two alternative $T_1(0)$ sites (**Fig 1.4** and its mirror image), related in a similar way to twinning on the Albite law [reflection across a (010) composition plane]. Diffusion of Al into $T_1(0)$ sites in albite occurs mainly in the orange band in **Fig. 1.5**. Intermediate microcline occurs naturally but its stability is doubtful.

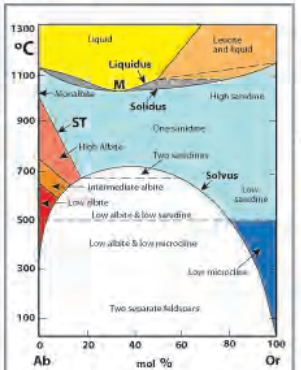

Fig 1.5[4] Stable equilibrium 'strain-free' phase diagram for An-free alkali feldspars with equilibrium Si-Al ordering, at atmospheric *P*.

1.5 Phase equilibria[6,7] Phase compositions in perthites and of pairs of feldspars growing simultaneously from magma or during metamorphism are defined by a ternary solvus surface (**Fig 2.5**) but principles can be illustrated using the binary system Ab-Or (**Figs 1.5, 1.6**). The solvus curve in **Fig. 1.5** is for separate, 'strain-free' or 'incoherent' feldspar phases with equilibrium Si-Al order[6]. (Feldspar pairs which share a common Si-Al-O framework lie on a coherent solvus. **Fig 2.1**). At low P_{H2O} (**Fig 1.5**) solidus and solvus do not intersect. A single feldspar is in equilibrium with all liquids, as in hypersolvus igneous rocks.

Elevated P_{H2O} (**Fig 1.6**)[6] lowers solidus *T* markedly, and *P* increases solvus *T* (by ~200°C GPa^{-1}) causing solidus and solvus to intersect at ~400 MPa. Two feldspars are in equilibrium with liquid at the solidus, as is the case in subsolvus igneous rocks. An in Af and Or in Pl will considerably increase the *T* at which the intersection of the solvus with the solidus occurs (**Fig 2.5**). Feldspars crystallizing during low *T* metamorphism and diagenesis are close to pure Ab and Or.

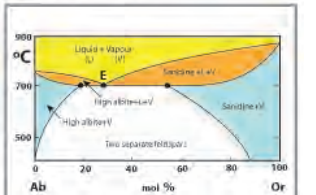

Fig 1.6[6] Metastable phase diagram for An-free disordered alkali feldspars at P_{H2O} 500 MPa. Two feldspars are in equilibrium with liquid at the eutectic E. All feldspars are disordered.

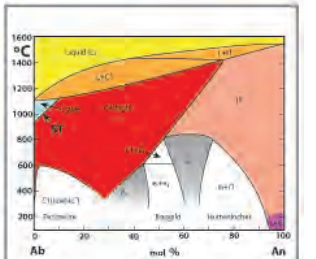

Fig 1.7[7] Phase diagram for Or-free plagioclase feldspars, showing liquidus and solidus curves at atmospheric *P* and probable subsolidus relationships in feldspars with equilibrium order.

In Pl (**Fig 1.7**)[7] the *T* of the liquidus-solidus loop is strongly dependent on P_{H2O} and also on the small amount of Or that all Pl contain. Strong compositional zoning, developed during crystal growth, often survives in Pl because Ca is coupled to Al and diffusion of T ions is slow.

Crystals with An-rich core are 'normally' zoned, those with more Ab-rich cores have 'reversed' zoning. Zoning is most common in crystals with >Ab_{40} because the gap between liquidus and solidus is larger and *T* are lower, so that zoning is not destroyed by diffusion.

The sub-optical peristerite, Bøggild and Huttenlocher intergrowths probably correspond with solvus curves that are conditional on Si-Al ordering. Breaks in the compositional range of metamorphic plagioclase are ascribed to these miscibility gaps.

FELDSPARS 2
Phase behaviour

The terminology of components and phases is given on Feldspars 1.

The first letter in the names of twin laws is capitalized.

2.1 Exsolution and phase behaviour. In a normal phase diagram **(Fig 1.5)** AF and PL form separate phases, each composed of homogeneous crystals. Na↔K exchange occurs between crystals when *T* changes. Exsolution textures do not form in either AF or PL.

In Nature this rarely happens. **Fig. 2.1** shows phase behaviour in an imaginary An-free system. The heavy lines trace the behaviour of the AF phase in an An-free subsolvus granite. In a real granite the presence of An will increase the *T* of the solvus curves considerably **(Fig. 2.5)**. On Fig 2.1 AF and PL crystallize simultaneously from magma on the strain-free solvus. Each behaves as a closed system during cooling. Coherent exsolution in AF begins at **B**, just below a coherent solvus, inside the strain-free solvus. Na↔K interdiffusion occurs within a continuous Si–Al–O framework leading to coherent film perthite **(Fig 2.3)**. Because of the different ionic radii of Na^{1+} and K^{1+} the crystal structure distorts at the interfaces of exsolution lamellae, leading to coherency strain. Exsolution is said to be 'strain-controlled'.

Fig 2.1 is a behaviour diagram[85]. The phases interact structurally with each other. Phase compositions, the shearing transformation ST, Si-Al ordering and related twinning, interact during coarsening giving rise to microtextures that vary with bulk composition **(Fig 2.2)**. Interfaces between phases and twins adopt orientations that minimize coherency strain energy.

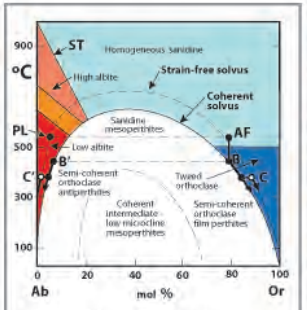

Fig 2. 1[85] Behaviour diagram for coherent and semicoherent An-free alkali feldspars.

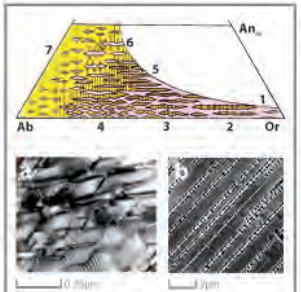

Fig 2.2[19] Cartoon (not to scale) showing variation in strain-controlled microtextures in slowly cooled alkali feldspars. Vertical lines are Albite twins in perthitic albite and PL. **(1)** Fully coherent lenticular film lamellae. **(2)** Semi-coherent straight film albite lamellae in orthoclase with misfit dislocations. SE SEM image **(b)** shows a (001) cleavage surface etched with HF. Paired black dots are the outcrops of nanotunnels that have formed on misfit dislocations, enlarged by etching. **(3)** Zig-zag intermediate microcline mesoperthite. **(4)** Braid mesoperthite. TEM image **(a)** shows Albite-twinned albite and zig-zag lamellae of low microcline. **(5)** Sinuous film mesoperthite. Straight examples have misfit dislocations. **(6)** Corrugated sanidine lenses in cryptoantiperthite, with tapering Albite twins propagating into PL matrix. **(7)** Sanidine platelets nucleated on Albite twin lamellae in PL.

2.2 Strain-controlled exsolution[19] In granites bulk AF ranges from ~Ab_5 to Ab_{30}. Strain-controlled albite film lamellae **(Figs 2.2, 2.3, 2.6)** form flat lenses in $(\bar{6}01)$ and become semicoherent when coherency strain is relieved by periodic misfit dislocations **(Fig 2.2b)**. These are an important factor in the dissolution and degradation of AF during weathering. The Or rich phase is often tweed orthoclase. In volcanic rocks the periodicity of fine-scale fully coherent lamellae in sanidine can be used to obtain cooling rates. An-poor AF in syenitic rocks (Ab_{50}–Ab_{70}) forms braid mesoperthite **(Figs 2.2, 2.2a, 2.4)** with zig-zag bands of microcline in $(\bar{6}\bar{6}1)$. In mesoperthites with >2% An (common in granulites) lamellae may be sinuous or straight and the Or rich phase is tweed orthoclase.

Phase behaviour of low PL **(Fig 1.7)** is uncertain. At low *T* a mixture of end-member albite and anorthite may be stable. The miscibility gaps then represent kinetically controlled coherent phase behaviour. The peristerite gap is conditional on ordering, the Baggild gap depends on ordering patterns which lead to breaks between $C\bar{1}/e_1$ or e_1/e_2 structures, and the Huttenlocher gap is a consequence of an $I\bar{1}\leftrightarrow e_1$ ordering transition. The $C\bar{1}\leftrightarrow I\bar{1}$ transition depends on long-range ordering. The $C2/m\leftrightarrow C\bar{1}$ and $I\bar{1}\leftrightarrow P\bar{1}$ transitions are rapid and depend on framework shearing.

2.3 Replacement reactions[11]. Coherency strain is often released during replacement reactions in aqueous fluids, at <500 °C. Phase compositions move onto the 'strain-free' solvus **(Fig 2.1,** points **C, C')**.The reactions lead to 'deuteric coarsening' of perthite **(Figs 2.3, 2.4)** by factors of as much as 10^3.The transformation of orthoclase to microcline often takes place during this replacement process.

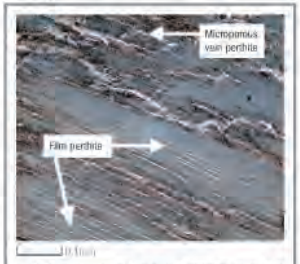

Fig 2.3 Strain-controlled film perthite, cross-cut by areas of turbid, replacement vein perthite. Shap granite. Optical, XP

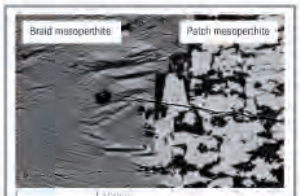

Fig 2.4 Microtexture in a single AF crystal in a syenite. Light grey microcline, dark grey albite. Black dots are micropores. Braid mesoperthite (left) has been converted into strain-free patch mesoperthite (right) by mutual replacement. Klokken syenite. Back-scattered electron image.

Textures produced by replacement reactions in aqueous fluids are common in feldspars. 'Mutual replacement' reactions are isochemical with respect to the bulk crystal and are driven by energy related to the release of coherency strain. In **Fig 2.4** the fully coherent braid mesoperthite has dissolved and reprecipitated as a patch perthite composed of strain-free low albite and microcline subgrains with sub-μm micropores between them, causing optical turbidity.

In Or-rich bulk compositions characteristic of granites **(Fig 2.3)** replacement reactions lead to turbid, coarsened vein perthite which may sometimes represent non-isochemical replacement. Fluid ingress is guided by nanotunnels which form by dissolution of the cores of misfit dislocations **(Fig. 2.2b)**.

Mutual replacement requires crystals to have constant bulk composition throughout a rock, but this is difficult to demonstrate. The hall-marks of replacement reactions are the development of micropores and very commonly of intracrystal subgrains of microcline and low albite with the [110] habit characteristic of the low-*T* feldspar varieties adularia (K-feldspar) and pericline (Na).

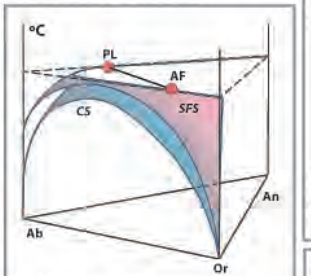

Fig 2.5 Strain-free *(SFS)* and coherent *(CS)* solvus surfaces in the ternary system Ab–Or–An. PL-AF is a tie-line on an isotherm that could be used for two-feldspar geothermometry.

2.4 Ternary equilibria and geothermometry[11]. Almost all natural feldspars are ternary solid solutions in the system Ab–Or–An **(Fig 2.5)**. Binary solvus curves **(Figs 1.5, 1.6 and 2.1)** are the intersection of a steep dome-shaped ternary solvus surface with the Ab–Or join. PL–AF tie-lines depend on *T* and less strongly on *P*. This forms the basis of two-feldspar geothermometry. *T* estimates are very strongly dependent on small amounts of An in AF and of Or in PL. The thermometer is independent of other components in rocks. Experimental data exist only for disordered, incoherent ternary feldspars *(SFS* in **Fig 2.5)** but the beginning of coherent exsolution in AF (at *CS*) is also likely to depend strongly on An.

2.5 Twinning and phase transitions[122]. Phase transitions and repeated twinning are interrelated in AF. 'Polysynthetic' twinning involves a large number of individuals related by the same twin law and occurs only in triclinic feldspars. Twins on the Albite law have composition planes parallel to the conspicuous (010) cleavage. Twins on the Pericline law **(Fig 2.6)** have an irrational composition plane (called the rhombic section) which lies in the plane of the *b*-axis, about which it rotates depending on composition and Si–Al ordering.

Twinning in anorthoclase[113] **(Fig 2.7)** develops during the shearing transition (ST, **Fig 2.1)**. It disappears rapidly and reversibly when the crystal is heated. As one region of the feldspar becomes triclinic on cooling across ST it is balanced by a corresponding triclinic region related to the first by a mirror operation. The overall *C2/m* symmetry of sanidine across the *m*-plane **(Fig 1.4)** is thus preserved.

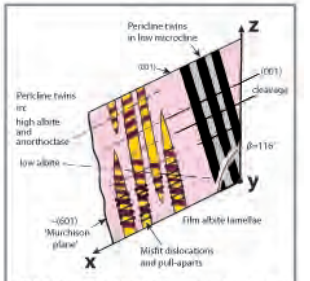

Fig 2.6 Orientation of film albite exsolution lamellae and Pericline twins in an alkali feldspar cleavage fragment lying on (010). Twins on the Albite law are parallel to (010) in all feldspars

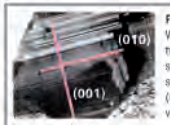

Fig 2.7 Anorthoclase[123]. When Albite and Pericline twins are visible they are sharply defined and straight. Both (001) and (010) cleavages are visible.

In microcline 'tartan' twinning[114] forms slowly during the ordering phase transition and persists for long heating periods at high *T*.

Fig 2.8 Microcline. Albite and Pericline twins appear spindle shaped and diffuse in (001). Only the (010) cleavage is visible. XP

Orthoclase[3] is monoclinic but has a diffuse fine-scale 'tweed' texture of partially ordered domains orientated like tartan twins. The texture cannot coarsen because the free energy of ordering is balanced by strain energy in domain walls. Twinned microcline often develops during fluid-feldspar reactions.

Fig 2.9 Orthoclase and microcline. Tweed orthoclase surrounded by microcline with irregular twinning.

Polysynthetic twinning in PL[115] forms during crystal growth, or in response to deformation. Growth twins have steps in composition surfaces, may terminate abruptly and change thickness independently of adjacent twins. Glide twins are lenticular or tapering, and occur in clusters in which thickness varies sympathetically.

©Mineralogical Society
Compiled 2009 from many sources by Ian Parsons, University of Edinburgh. Sources and supporting information corresponding with the numbered footnotes are given in Parsons I (2010) Mineralogical Magazine Vol 74, 529-551
Designed by www.keatsgraphics.co.uk

provide comprehensive review papers. Volume 2 of the Mineralogical Society of America's 'Reviews in Mineralogy' series, *Feldspar Mineralogy* (Ribbe, 1983), is useful but out of print. The present notes do not deal with optical methods of identifying feldspars, which are described in most general mineralogy text books, and comprehensively by Smith and Brown (1988), who also cover X-ray diffraction methods.

Feldspars I: Nomenclature, structure and phase relationships

1. Colour and turbidity

There are four interconnected aspects of feldspar colour: (a) the intrinsic absorption colour of the feldspar itself, when in the form of perfect, unmodified crystals and fragments; (b) colours that are produced by scattering of light by planar feldspar microstructures, collectively called 'iridescence'; (c) translucency and turbidity caused by the presence of μm-sized micropores, often containing fluid; (d) colour imparted by mineral inclusions, most commonly as tiny particles contained in pores. These are sometimes aligned causing a play of light called 'schiller'. Hofmeister and Rossman (1983) provided a comprehensive review of feldspar colour. Later data have been added by Smith and Brown (1988) and Deer *et al*. (2001).

Feldspars in categories (a) and (b) are 'unaltered' or 'fresh' in petrologists' parlance. Sanidine in volcanic rocks is often glass clear and colourless and glass-clear 'gem-quality' feldspar is sometimes found in pegmatites. Structural Fe^{3+} causes a yellow colour, as in the gem-quality orthoclase crystals from Madagascar. A strong green colour often correlates with high Pb content (see Hofmeister and Rossman, 1983, for detail). A commonplace plutonic rock in which the feldspar is clear in small fragments or thin section is the variety of syenite called larvikite, used as an architectural stone because of the striking blue iridescence of its AF. The feldspar is a cryptomesoperthite (Sheet 1, Sec. 3) and the iridescence is caused by coherent scattering of light by exsolution lamellae similar to those shown in Sheet 2, Fig. 2.2a. The physics of iridescence is discussed by Smith (1974, vol. 1, p. 377). He recommends that the term iridescence should be used explicitly for this type of optical effect and the term schiller reserved for light scattered by visible inclusions of other minerals. In massive lumps, feldspar in larvikitic syenites ranges from light blue-grey to dark bottle green, almost black. Comparable non-turbid feldspars in granulite-facies gneisses and charnockites are often green but do not show iridescence because of the coarser spacing and irregularity of their exsolution textures. In Or-rich AF silvery or blue iridescence (seen in the gem variety moonstone) is caused by lamellar intergrowths similar to those in Sheet 2, Fig. 2.2b, but on a finer scale.

Iridescence occurs in some PL in the peristerite, Bøggild and Huttenlocher ranges (Sheet 1, Fig. 1.7), again caused by Bragg diffraction by lamellar intergrowths. Smith and Brown (1988, Section 19.3) discuss the origin of the iridescence in detail. In peristerites and Huttenlocher intergrowths it is blue but in the Bøggild range (called 'labradorescence') the colour changes through the spectrum from blue in An_{48} to red at An_{59}, as the lamellar periodicity increases from ~80 to 250 nm.

Most feldspars are turbid, to variable extents. Turbidity is a non-trivial feature that is an important marker of widespread replacement reactions in fluids permeating large volumes of the crust (Parsons, 1978; Putnis 2002, 2009) (see Sheet 2, Sec. 2.3). Brownish turbidity in thin section is a convenient way of distinguishing feldspar from quartz. Folk (1955) showed that turbidity is mainly caused by large numbers of 'vacuoles', often fluid-filled. They are now usually called 'micropores'. Montgomery and Brace (1975) used SEM to demonstrate their character in PL, and Worden *et al*. (1990) used TEM to demonstrate their connection with pervasive recrystallization of AF. Walker *et al*. (1995) reviewed AF microporosity in general. The largest pores are >2 μm long, the smallest a few nm, and there may be 10^9 pores mm^{-3} and porosities as high as 4.75 vol.%. Because of their small size, fluids in feldspar micropores have been less studied than those in quartz, but Johnson and Rossman (2004) calculated that in the upper crust the amount of water they contain is roughly the same as in all hydrous minerals together. More intensive alteration of AF leads to replacement by kaolinite, and can ultimately lead to perfect pseudomorphs (Putnis, 2009, fig. 2).

The colour of red and pink turbid feldspars has long been inferred to be due to sub-microscopic inclusions of hematite. In rare instances these are large enough for their platy morphology and hexagonal shape to be visible in a petrographic microscope (Smith 1974*b*, Section 20.4). The phenomenon of 'schiller' or 'aventurization', a

play of light and colour, is caused by reflections from parallel flakes, usually of hematite. The presence of sub-optical hematite in micropores in red and pink feldspars was demonstrated using TEM by Putnis *et al*. (2007) who stressed that red colouration is a direct indicator of pervasive and large-scale sub-solidus recrystallization in granitic rocks (see Sheet 2, Sec. 3 and Note 10). Worden *et al*. (1990) showed, using TEM, that white turbid AF contained titanomagnetite and (rarely) clay minerals in micropores. Walker *et al*. (1995) studied a variety of igneous rocks and showed that although most pores did not contain solids those that did contained phases with a range of chemical compositions, sometimes distinctive of individual intrusions. The nature of solid phases in feldspar micropores deserves intensive study using modern techniques.

2. Repeated fine-scale twinning

Often called 'polysynthetic' twinning, it can occur only in triclinic feldspars and is almost always developed over a range of dimensions. Feldspar twinning is discussed in detail by Smith and Brown (1988, chapter 18). The names of twin laws should be capitalized. It arises because the feldspar structure is pseudosymmetric. The triclinic forms depart only slightly from monoclinc geometry. (010) is close to being a mirror plane (thus it is termed a pseudo-mirror-plane) and the normal to (010) is a pseudo-two-fold axis. Although each twin is triclinic (see Note 12) the sandwich of alternating 'left'–'right' sheets has overall monoclinic symmetry. In hand specimens of plagioclase, repeated twinning on the Albite law can sometimes be seen with the naked eye, more often with a hand lens, and can be a useful way of distinguishing plagioclase from alkali feldspar in the field. Repeated twinning in microcline is rarely visible in hand specimen. (See Sheet 2, Sec. 5 for discussion of the origin of twinning).

3. Components and phases

It is important to use terms rigorously when describing feldspars. For example, the word 'albite' can refer to the *component*, the *mineral* albite, a *feldspar phase* rich in the albite component in an intergrowth, or a *twin law* (see 2, above). Use of the abbreviations Ab, An and Or is a fool-proof way of denoting *components*. Where a feldspar close to pure $NaAlSi_3O_8$ occurs as single crystals (as in albite schists) or overgrowths (for example during diagenetic albitization) it is correctly called albite. When coexisting with an Or-rich feldspar in a perthitic intergrowth, it is best to refer to the 'Ab-rich phase', since its composition is strictly unknown, although it is usually close to end-member albite, and 'albite lamellae' is acceptable in perthites like Fig. 2.3. The K-rich member of a perthitic intergrowth is best called the 'Or-rich phase', because its composition and structural state (sanidine, orthoclase, microcline or mixtures thereof) are often not known. Feldspar pairs growing from magma or during high-T metamorphism are usually simply called the plagioclase (PL on these sheets) and alkali feldspar (AF) phases. Strictly speaking the boundary between PL and AF in a phase equilibrium sense is a curved line, called the *critical solution* or *consolute* line, which corresponds with the top of the ternary feldspar solvus, where pairs of feldspars (PL and AF on Fig. 2.5) on each isotherm come to have the same composition. This is an important consideration in two-feldspar geothermometry (Brown and Parsons, 1981) but the critical solution curve is sensitive to P and at present too poorly defined to be used for nomenclature. See Brown (1993).

Care is required when describing plutonic Or-rich AF. $KAlSi_3O_8$ is the 'orthoclase component', abbreviated to Or, but 'orthoclase' also has a specialized structural meaning, a relatively ordered but optically monoclinic Or-rich feldspar with $2V > \sim 50^{o}$ and a 'tweed' microstructure at the TEM scale (see Fig. 2.9 and Note 5). It is not a stable phase at any T. In these notes Or is used for the component and the term 'orthoclase' restricted to its specialized meaning. The term 'alkali feldspar' refers to the entire field on Fig. 1.2. The most satisfactory generic term for Or-rich feldspars that have not been subject to careful optical, X-ray or TEM work is 'K-feldspar'. Depending on context (for example, when describing a rock in the field) this term usually refers to the bulk crystal including perthitic albite. The bulk K-feldspar is then made up of Ab- and Or-rich phases. Many K-feldspars in plutonic rocks are mixtures of orthoclase and microcline (Fig. 2.9).

Finally, it is most important, when dealing with microbeam analyses, to state whether the analysis is a bulk analysis of a crystal that is an intergrowth, or an analysis of one or other of the phases in an intergrowth. In application of two-feldspar geothermometry (Sheet 2, Sec. 4) to

obtain *T* of magmatic or metamorphic growth, it is necessary to obtain bulk AF analyses. Analysis with a stationary small-diameter beam can provide a crystal bulk composition of intergrowths only when they have a periodicity considerably smaller than the beam and for regular film or braid microperthites (Figs 2.3, 2.4) either a defocused beam or a traversing method must be used to obtain bulk composition. It is difficult to obtain reliable bulk analyses of coarse vein and patch perthite (Figs 2.3, 2.4). The situation is further complicated by the possibility that the dissolution–reprecipitation reactions that produce these relatively coarse, irregular perthites are non-isochemical (see Sheet 2, Sec. 3 and Note 10). The bulk composition of a strain-controlled intergrowth (Sheet 2, Sec. 2) provides the most reliable guide to the composition of the AF phase at the time of crystal growth, because once they have formed, strain-controlled intergrowths cannot survive fluid–feldspar reactions (Brown and Parsons, 1993). With rare exceptions intergrowths in PL are at scales well below the analysed volume of a focused electron microprobe beam.

4. Nomenclature

Figure 1.2 is slightly modified from Smith and Brown (1988, fig. 9.2). There is no official International Mineralogical Association nomenclature for feldspars. Most fields on Fig. 1.2 are defined by chemical composition simply for convenience and by long-standing convention. The only exception is the field of anorthoclase, which extends slightly into the PL field. Feldspars in the anorthoclase field are triclinic at 25ºC, but invert instantaneously and reversibly to monoclinic symmetry as *T* is increased, at the shearing transformation (ST in Figs 1.5 and 1.7). The boundary of the anorthoclase field in AF corresponds with 25ºC, the boundary in PL with ~1100ºC. See Kroll and Bambauer (1981). Sanidine is always monoclinic and has variable degrees of Si–Al order (see Note 5 for an explanation of order–disorder in feldspars). However, below ~500ºC the stable form of Or-rich K-feldspar is triclinic, ordered microcline. Ordering is a relatively slow process (see Sheet 1, Sec. 4 and Note 5) so that monoclinic sanidine often persists metastably at 25ºC. All PL are triclinic at 25ºC irrespective of degree of order.

At low *T* (Fig. 1.3) solid solution in ordered feldspars is extremely limited and most crystals are intergrowths. In AF, relationships are uncontroversial and the subdivision of perthitic intergrowths into perthite *sensu stricto*, mesoperthite and antiperthite is simply a function of bulk composition. Figure 1.3 is based on Smith and Brown (1988, fig. 1.6*b*) with the addition of defined boundaries to the mesoperthite field at one-third intervals on the Ab–Or join. The term 'mesoperthite' is often reserved for the coarse, sinuous intergrowths found in feldspars from granulite-facies rocks, but this is too restrictive and the term used should be based only on bulk composition. It should also be noted that the word 'perthite' applies to the *totality* of the intergrowth, and includes both Ab- and Or-rich phases. In petrographic descriptions of granitic rocks the albite lamellae alone are often called 'perthite' but this is incorrect. What appears to be Or-rich feldspar at the optical scale is often itself cryptoperthitic, even in plutonic rocks (e.g. Lee *et al*., 1995), including granitic pegmatites (Parsons and Lee, 2005). The common belief that cryptoperthites occur only in rapidly cooled rocks is a myth. Cryptoantiperthites (Brown and Parsons, 1988) are rarely reported but may be common.

Phase relationships in ordered PL (low-PL) are much more complex (see Fig. 1.7 and Note 7) than in AF, but from the standpoint of nomenclature for routine petrography the three miscibility gaps can be ignored and the familiar names for compositional ranges used (Fig. 1.2). Peristerites are occasionally visible in a petrographic microscope (see Smith and Brown, 1988, fig. 19.28) but usually require TEM methods. Bøggild and Huttenlocher intergrowths always require TEM. Iridescence (see Note 1) is the only simple guide to the presence of these intergrowths. The *e*-structure (see Note 7) requires single crystal XRD or TEM methods.

5. Crystal structure and symmetry

The arrangement of tetrahedra in the framework of a feldspar, sanidine, was first envisaged by W.H. Taylor on Christmas Day, 1932 (Taylor, 1933). Figure 1.4 is slightly modified from Ribbe (1983), and is based on Taylor's work and that of Laves (1960). Oxygen is not shown in the diagram, and only two chains of Si^{4+} and Al^{3+} ions are indicated. Si or Al occupy all positions where lines in the framework join (*T* sites), all surrounded by tetrahedra of O^{2-}. Some short linkages from tetrahedral nodes are with unit cells

above or below the unit cell outlined by the rectangle in the centre of the drawing, emphasizing that although feldspar structures can be usefully simplified into chains and sheets (like Fig. 1.4), the structure is a three-dimensional framework. Because (001) is not at right angles to *c* (the lattice angle β is close to 116º) the *c* axis in the drawing is inclined, indicated by a tapered arrow. In this projection Si and Al tetrahedra form 10-membered rings around the *M* site, which has a complex shape to which it is difficult to apply simple ideas of coordination number. Smith and Brown, (1988, chap. 14) discuss trace and minor-element substitutions in feldspars, and provide a wealth of chemical data.

In most feldspars at high *T* all possible positions for Al and Si (called 'equivalent sites') are occupied at random by Si and Al ions, and the feldspar is said to be *disordered*. Ignoring for a moment the colouring of T ions in Fig. 1.4, there is a 1-in-4 chance of encountering an Al on any *T* site. This is the situation in high sanidine. However, the equivalent sites are of two types, labelled T_1 and T_2 in Fig. 1.4. The sites occur in pairs which in monoclinic feldspars (Fig. 1.4) are related by mirror symmetry. T_2 sites are closer together than T_1 and have a different relationship to the *M* cation. As *T* decreases T_1 sites become energetically favourable for Al, which diffuses from T_2 sites into T_1. In principle, all Al can occupy T_1 sites, with none remaining in T_2. There is then a 1-in-2 chance of finding an Al on any T_1 site. If T_1 sites are occupied at random, the *partially ordered* structure retains overall monoclinic symmetry. This type of ordering is said to be *non-convergent*. The most highly ordered low-sanidine crystals may approximate to this structure.

However, in any set of four equivalent sites there is only one Al, so that even in the hypothetical case when all Al is in T_1 there is a local loss of mirror symmetry, as in the $T_1(0)$, $T_1(m)$, $T_2(0)$, $T_2(m)$ ring in the centre of Fig. 1.4. A second type of ordering (*convergent ordering*) occurs in which Al becomes concentrated in the $T_1(0)$ site over large regions of the structure. There are two ways in which this can happen. In albite, framework ordering takes place in a structure which is triclinic because of the shearing transformation (ST, Fig. 1.5). The T site in which all Al will be sited in low albite [$T_1(0)$, Fig. 1.4] is defined as soon as an Ab-rich feldspar crosses ST. In this case Fig. 1 is distorted slightly (in a 'right-' or 'left-handed' sense) from monoclinc symmetry, and the ordering phase transition can occur by a continuous process. Convergent ordering in Ab-rich AF occurs mainly in the orange band on Fig. 1.5, the high−low albite phase transition. Intermediate albite, with its Si−Al order increasing with falling *T*, is stable in this band.

The process is different in the case of monoclinic sanidine, where the Al has two 'choices' of T_1 site, related by symmetry [labelled $T_1(0)$ and $T_1(m)$ in Fig. 1.4, although in a monoclinic framework they are indistinguishable]. Al thus concentrates in T_1 sites, by diffusion from T_2, while the crystal maintains monoclinic symmetry. However, because in any set of four equivalent T sites there is only one Al, mirror symmetry must be lost locally, and the position of the Al *defines* which of the two T_1 sites can be labelled $T_1(0)$. As there are two choices, small 'left' and 'right' triclinic ordering domains develop, where Al is in the same equivalent site in a small number of adjacent unit cells. Each corresponds with a slightly distorted version of Fig. 1.4 and its mirror-image. These embryos give rise to a very fine-scale modulated structure known as 'tweed' (Fig. 2.9) which is composed of alternating domains, orientated like Albite and Pericline twins in microcline, each domain being only a few unit cells thick. This is the microstructure of orthoclase. Orthoclase is optically monoclinic, with large 2V (>50º), and is monoclinic in powder XRD patterns, but in single crystal XRD and electron diffraction patterns individual Bragg diffraction spots are streaked normal to the tweed modulations. Tweed texture is not unique to orthoclase. It develops in many crystalline materials undergoing phase transitions in which loss of point group symmetry results in transformation twinning in the low-*T* form, and also in crystals undergoing the exsolution process known as spinodal decomposition (see Note 9). See Putnis and Salje (1994) for a general review of tweed.

The nature of orthoclase was finally established using high-resolution TEM by Eggleton and Buseck (1980). They calculated that the free energy released by Si−Al ordering was balanced by strain energy acquired in the walls of the triclinic domains constrained to maintain an average monoclinic shape. Thus, further ordering is blocked. The orthoclase is therefore in a metastable equilibrium that will persist indefinitely unless some 'unzipping' event such as

reaction with fluids or deformation can occur (Brown and Parsons, 1989; Note 6c). Orthoclase should therefore not appear on phase diagrams (Fig. 1.5) but is appropriate on behaviour diagrams (Fig. 2.1).

6. Phase relationships for the Ab–Or join

Feldspars furnish numerous examples of metastable equilibrium, and of intra-crystal reactions that occur at very different rates. Figures 1.5 and 1.6 were chosen to illustrate three important features of the AF system: (a) the effect of P_{H_2O} in causing the intersection of the solidus with the solvus. (b) The difference between an inferred stable equilibrium phase diagram (Fig. 1.5) which is based in part on natural starting materials and evidence from field studies, and a second phase diagram (Fig. 1.6) which is based entirely on laboratory experiments but is, in part, metastable. (c) The currently accepted relationships of the AF polymorphs (Fig 1.5).

(a) Solvus–solidus relationships

Figures 1.5 and 1.6 are *conventional phase diagrams*. When two feldspar phases are present they form separate crystals or occur in perthitic intergrowths in which the Si, Al–O framework is discontinuous or '*incoherent*'. Below the solidus, coexisting solid phase compositions are defined by solvus curves which are said to be '*strain free*'. In reality, in most natural circumstances, exsolution leads initially to perthitic intergrowths which share a continuous Si, Al–O framework and are said to be '*coherent*' (Sheet 2, Sec. 1). In such intergrowths the different cell dimensions of the Ab- and Or-rich phases lead to coherency strain which varies with bulk composition. Coherent phase relationships cannot be depicted on a conventional phase diagram and a behaviour diagram such as Fig. 2.1 is required.

Figure 1.5 is for atmospheric *P*. The solidus and liquidus curves are from Schairer (1950). Melts of AF composition are difficult to crystallize in the absence of water and the curves are approximate. The liquidus and solidus touch at a *binary minimum*. At low *P* the liquidus phase for Or-rich liquids is the feldspathoid leucite, $KAlSi_2O_6$, and Or-rich feldspars melt incongruently to leucite and an SiO_2- and Na_2O-rich liquid. As P_{H_2O} increases the field of leucite shrinks and disappears for compositions on the Ab–Or join at 260 MPa. A useful review of the phase relationships of alkali feldspars and leucite was provided by Henderson (1984). The solidus is well above the solvus so a single alkali feldspar solid solution, either Ab- or Or-rich, is the final product of crystallization of all liquids, the situation, in simplified form, in *hypersolvus* igneous rocks. The solvus in this diagram is for feldspars with an equilibrium degree of Si–Al ordering (see *b*).

Figure 1.6 shows phase relationships at P_{H_2O} 500 MPa. The liquidus and solidus curves are from Morse (1970, fig. 2) and the solvus curve is the synthesis curve of Smith and Parsons (1974) obtained at 100 MPa but here moved upwards by 22ºC/100 MPa, the *P* dependence recommended by Hovis *et al*. (1991). Compared with Fig. 1.5 the solidus has moved down in *T* by >300ºC and the solvus has moved up by ~90ºC so that the two curves intersect. Note that the depression of the solidus depends on P_{H_2O} because water, dissolved in the silicate liquid, is a reactant. The elevation of the solvus depends only on *P*, because the solubility of water in feldspar is insignificant. The liquidus and solidus now meet at a *eutectic* E where two feldspars are in equilibrium with liquid. Again in simplified form, this is the situation in *subsolvus* igneous rocks. Morse (1970) estimated that solidus and solvus would intersect at P_{H_2O} of 425 MPa. However the effect of the An component on the ternary solvus (Fig. 2.5) is very large so that many subsolvus granites owe their feldspar assemblage as much to small concentrations of An as to high P_{H_2O}. An important feature of the alkali feldspar solvus is its asymmetry, steeper on the Ab-rich limb than on the Or-rich limb. This is even more marked on slices of the ternary solvus (Fig. 2.5) sub-parallel to the Ab–Or join. The asymmetry accounts for the common petrographic observation that K-feldspars coexisting with PL are often visibly perthitic (e.g. Fig. 2.3) while the PL is not visibly antiperthitic.

(b) Stable and metastable solvus curves

The subsolidus part of Fig. 1.5 is slightly modified from fig. 8a in Brown and Parsons (1989) and is an attempt to depict stable equilibrium phase relationships that include Si–Al ordering (see Note 5). In principle (although never in practice, see Note 8), an AF crystallized above the solvus (in a hypersolvus rock) will begin to exsolve when the feldspar encounters a strain-free solvus curve (Fig. 1.5) for feldspars with equilibrium order. Exsolution on the strain-free solvus leads to two structurally

separate (or 'incoherent') feldspar phases, perhaps in an incoherent perthitic intergrowth. When AF and PL crystallize simultaneously (in a subsolvus rock) both feldspars will have stable equilibrium compositions (on the solvus curve) and stable equilibrium degrees of Si−Al order. Again, in principle but not usually in practice, the AF and PL phases will, on cooling, exchange alkali ions as their compositions diverge and ordering continues. Perthitic intergrowths will not form.

A solvus for feldspar pairs with an equilibrium degree of order cannot be obtained by direct synthesis because ordering is too slow. It is necessary to start with natural feldspars of known order and to exchange Na^+ and K^+ between them. Alkali exchange is much faster than Si−Al disordering so that solvus curves for different degrees of order can be obtained. Solvi for feldspars with fully and partially ordered frameworks were obtained by Bachinski and Müller (1971), and Müller (1971). Brown and Parsons (1984*a*) constructed the solvus in Fig. 1.5 from these curves and from a disordered solvus obtained by direct synthesis by Smith and Parsons (1974). It is therefore an approximation to the true stable equilibrium solvus. Figure 1.6 was obtained by direct synthesis and all feldspars are disordered (there may be some order on the Ab-rich limb) so the solvus represents metastable equilibrium with respect to ordering. The ordered solvus is at ~100ºC higher *T* than the disordered solvus; the significance of this difference for two-feldspar geothermometry is discussed in Note 11.

(c) Phase transitions

Figure 1.5 shows phase transitions in the Ab−Or system. Above ~1000ºC all disordered AF are monoclinic when *observed* at *T*. When cooled, and irrespective of cooling rate, Ab-rich alkali feldspars adopt triclinic symmetry at the *shearing transformation*, ST (also called the *displacive* transformation). The transformation is instantaneous and reversible; the monoclinic form cannot be quenched. It does not involve breaking of bonds in the Si, Al−O framework, only spontaneous shearing of the framework involving changes in the relative tilt of tetrahedra. The cell angles α and γ depart continuously from 90º as a feldspar is cooled through the phase transition. If AF_{SS} are cooled sufficiently rapidly (quenched) from *T* above the solvus, exsolution does not occur and the metastable extension of the line ST can be studied at or below 25ºC. Or-bearing feldspars below this line are called *anorthoclase* (see Fig.1.2). The transformation was first studied experimentally by MacKenzie (1952) using high-*T* XRD. For fully disordered feldspars it intersects the 25ºC line at ~$Ab_{67}Or_{33}$, but it is sensitive to framework order if cooling is slow (Smith and Brown, 1988, fig. 7.13) and moves towards Or if the feldspar is partially ordered, as depicted in Fig. 1.5. The slope of ST is based on Kroll *et al*. (1980). The small monalbite field extends to about An_{10} on the Ab−An join (Fig. 1.7, labelled *C*2/*m*). In practice, high-*T* magmatic liquids do not crystallize feldspars in the monalbite field and Ab-rich feldspars in plutonic igneous and metamorphic rocks crystallize below ST.

High, intermediate and low albite are all triclinic, $C\bar{1}$, but vary in cell parameters, most markedly in the cell angles α and γ, as a result of ordering of Al onto the $T_1(0)$ tetrahedral site (Fig. 1.4 and Note 5). The '*structural state*' can be obtained readily from refined cell parameters or simply from the splitting of pairs of XRD peaks which are sensitive to the cell angles, such as $131-1\bar{3}1$ and $111-1\bar{1}1$. Mackenzie (1957) showed that a continuum of partially ordered albites could be made at different *T*. High albite formed initially in all experiments and then ordered with time. It is not clear whether crystals growing from magma behave in this way but it is possible that crystals growing slowly from melt or during metamorphism achieve equilibrium order as they grow. Goldsmith and Jenkins (1985) reversed the high−low albite transition using ordered and disordered starting materials at *P* from 1.7 to 1.9 GPa. Similar ordering behaviour occurs at low *P* (Brown and Parsons, 1989, fig. 1). Equilibrium order in high albite changes slowly and approximately linearly with *T* until slightly above 700ºC (at low *P*, Fig.1.5), then much more rapidly down to ~650ºC, below which changes are small. The intermediate albite band on Fig. 1.5 (from Brown and Parsons, 1989, fig. 6) represents the stage when most convergent ordering occurs (Note 5). At high *P* (1.8 GPa, Goldsmith and Jenkins, 1985) the high−low transition takes place at 30−70ºC higher *T*, and over a wider *T* interval. It is generally agreed that intermediate albite can exist as a stable phase, although it is uncommon because in most geological situations it will order further during slow cooling.

The two forms of Or-rich feldspar found in plutonic rocks, monoclinic orthoclase and triclinic microcline, are conventionally distinguished because of the distinctive 'tartan' twinning of

the latter (Fig. 2.8). At the sub-optical scale the relationship is more complex (Fig. 2.9) and tweed orthoclase and tartan microcline often occur together. Provided the composition of an alkali feldspar is known, the proportion of Al in T_1 sites (a measure of the degree of non-convergent order, see Note 5) can be obtained accurately by measuring 2V and taking account of the orientation of the optic axial plane, which is (010) in high sanidine and normal to (010) in low sanidine (Su *et al*. 1986). Ordering in sanidine was studied experimentally by Kroll and Knitter (1991). 'Steady state' degrees of order were reached in <100 days at 750ºC and would be reached after several years at 650ºC. This is slower than ordering in albite; fully ordered low albite was obtained after 14 days at 350ºC by Martin (1969). However, attempts to synthesize microcline at elevated *T* in its stability field below ~500ºC have been unsuccessful because the feldspar becomes 'stranded' with the tweed microtexture of orthoclase (Note 5 and Fig. 2.9) and the transition of sanidine to microcline has never been achieved experimentally. The only direct synthesis of microcline was reported by Flehmig (1977) in hydroxide gels held at 20ºC and atmospheric *P* in alkaline Na-Ca-K chloride solutions for 90 days, essentially diagenetic conditions.

In the absence of direct experimental evidence the thermodynamic character of the low sanidine → microcline transition (supposing that the problem of tweed formation could somehow be sidestepped), remains controversial. Brown and Parsons (1989, figs 6 and 8) considered it to be continuous, with a narrow band of stability of intermediate microcline analogous to that of intermediate albite (Fig. 1.5). This was based mainly on a compilation of largely unreversed experiments and the observation that intermediate microcline occurs, albeit rarely, in Nature (Note 9). The experiments suggest that at low *P* the monoclinic→triclinic symmetry change occurs mainly in the range 550−450ºC, and the boundary of the microcline field has been placed at 500ºC in Fig. 1.5. Carpenter and Salje (1994) carried out an analysis of the experiments of Kroll and Knitter (1991, see preceding paragraph) using the Landau theory of phase transitions and concluded that the transition was discontinuous (first-order). It is possible to synthesize both iron microcline ($KFeSi_3O_8$) and gallium microcline ($KGaSi_3O_8$) (Taroev *et al*., 2008) and the phase transition from Fe- and Ga-sanidine forms appears to be first-order. In the light of these studies no field for intermediate microcline is shown in Fig. 1.5 although in the writer's view its absence is by no means certain. Like orthoclase, intermediate microcline certainly has a place on a behaviour diagram (Fig. 2.1 and Notes 8, 9).

The temperature of the sanidine−microcline transition has also been estimated from the conversion of microcline to orthoclase in the contact aureoles of igneous intrusions, most recently by Kroll *et al*. (1991). They studied the conversion of detrital K-feldspar grains in quartzite near the contact of the Ballachulish granite in western Scotland. These grains were converted to tartan-twinned low microcline during Caledonian regional metamorphism, heated in the thermal aureole to produce, by inference, sanidine, which then ordered during cooling to produce tweed orthoclase and in places irregular, intermediate microcline. On the basis of a heat-flow model of the intrusion provided by Buntebarth (1991) they concluded that the microcline−sanidine transformation was at 480±20ºC, a value adopted by Carpenter and Salje (1994) in their Landau analysis. An interesting insight into ordering rates in K-feldspar (which are often stated in text-books to be extremely slow) was provided by McDowell (1986) who showed that low albite and low microcline are growing in real time in the Salton Sea geothermal field at measured borehole *T* in the range 360−250ºC. The Salton Sea system has been active for only ~16,000 y.

In detail the mechanism of the orthoclase–microcline transition is poorly understood. Microcline can develop from orthoclase following discontinuous dissolution−reprecipitation reactions in igneous rocks (e.g. Lee *et al*. 1995, figs 12, 14, 15) or during retrograde reactions in granulites (e.g. Waldron *et al*., 1993, fig. 2). In both these examples microcline forms well-defined subgrains in deuterically altered (Note 10) regions of orthoclase crystals. The details of the reprecipitation process are unknown and it is not clear how the intersecting 'tartan' Albite and Pericline twins develop in the new microcline. This so-called 'M-twinning' (which has overall monoclinic symmetry, although individual twins are triclinic) is conventionally taken to indicate formation from a monoclinic parent crystal, as originally proposed by Laves (1950). Waldron *et al*. (1993) deduced that the reactions in the granulites occurred at <350ºC at which *T* ordering by Si−Al interdiffu-

sion in a disordered parent would be extremely slow. When a dissolution–reprecipitation reaction can be supported by other evidence (as in Waldron *et al*., 1993) the tartan twinning in microcline is often irregular (a common style of twinning called 'irregular microcline' by Bambauer *et al*., 1989). Figure 2.9 (from Fitz Gerald and McLaren, 1982) is an excellent example of a crystal composed of tweed orthoclase and irregular microcline. It is not unreasonable to suppose that the texture in Fig. 2.9 arises as a result of an incomplete dissolution–reprecipitation reaction, but the textural evidence is not unequivocal.

Bambauer *et al*. (1989) studied the development of orthoclase and microcline in regional metamorphic rocks in the Swiss Alps and in the contact aureole of the Ballachulish granite. Orthoclase, irregular- and regular-microcline occurred together within single crystals. Ordering (based on estimates of Al in $T_1 0$ obtained from cell parameters) increased progressively from orthoclase to regular microcline, but Bambauer *et al*. did not venture any explanation for the intimate mixture of the three types of K-feldspar. There is a strong tendency for microcline to be the K-feldspar in the most chemically evolved members of intrusive igneous sequences, with orthoclase in less evolved members (Parsons and Boyd, 1971) an observation consistent with a role for water in the phase transition. What is much less clear is the mechanism of formation of the more regularly twinned varieties of microcline. Examples are given by Fitz Gerald and McLaren (1982). Some (e.g. their fig. 12) appear to be regularly organized orthoclase–microcline intergrowths, suggesting a continuous, diffusion controlled process involving coarsening of a tweed precursor. Harker (1954, 1962) showed that microcline developed at the expense of orthoclase in progressively more deformed acid orthogneisses. There is an urgent need for a systematic study of the microtextures of microcline in a range of well defined geological contexts.

7. Phase relationships for the Ab–An join

Figure 1.7 is a slightly amended version of fig. 6 from Carpenter (1994). The liquidus–solidus loop at atmospheric *P* was determined by N.L. Bowen (1913) working at the Geophysical Laboratory in Washington, D.C. It is a foundation work in experimental mineralogy, introducing the quenching method, locating the liquidus and solidus curves of a silicate solid solution for the first time and clarifying the concepts of 'isomorphous series' and 'solid solution'. The high *T* reached, up to 1550ºC for pure anorthite, in a platinum-wound furnace maintained at constant *T* (±2ºC) by continuously adjusting a resistance by hand, was state-of-the art science a century ago. The charges were quenched by dropping them into a dish of mercury. Bowen was not able to crystallize Ab-rich compositions near the solidus, which is therefore based on the beginning of melting of natural albite and oligoclase. Like the Ab–Or join the PL system is strongly sensitive to P_{H_2O}. The liquidus at 500 MPa was determined by Yoder *et al*. (1957); the most reliable determination of the solidus at this *P* was provided by Johannes (1979). Johannes (1994) provided an interesting overview of the important topic of partial melting of PL.

The most recent review of sub-solidus phase relationships of PL is that by Carpenter (1994). In high-*T* PL they are uncontroversial, with complete solid solution between Ab and An. The changes in space group, $C2/m$–$C\bar{1}$–$I\bar{1}$, do not lead to immiscibility. The $C2/m$–$C\bar{1}$ transition is caused by framework shearing (Note 6c) and the $C\bar{1}$–$I\bar{1}$ transition marks a change from a disordered high albite structure to an ordered anorthite structure (see below). The phase relations in low PL are much less well understood, and the way the transition lines meet and their relationship to the miscibility gaps in Fig. 1.7 is speculative. Strictly speaking Fig. 1.7 is probably a behaviour diagram (see Sheet 2, Sec.1 and Note 8). The apparent breakdown of single crystals of PL to albite + anorthite mixtures in metamorphic amphibolites (e.g. Wenk, 1979) and other instances of breaks in metamorphic PL, are consistent with complete immiscibility at low *T*, near end-member anorthite and albite being the only stable plagioclase feldspars. Such instances are rare, however, and most plutonic PL occurs as intergrowths, as depicted in Fig. 1.7, of largely unexplored petrogenetic significance.

The peristerite, Bøggild and Huttenlocher intergrowths are coherent, and can be described by solvus curves which are said to be 'conditional' on Si–Al ordering (see Note 5). As in many AF, the microtextures seen using TEM [see Carpenter (1994) and Smith and Brown (1988) for many variations] are often consistent with development by spinodal decomposition (see Note 9), but the fundamental driving forces for

exsolution in the AF and PL solid solutions are very different. In AF the driving force is primarily the different ionic radii of Na^+ and K^+ (see Sheet 1, Sec. 4) which impose large local strains on the Si−Al framework. If an homogeneous sanidine solid solution is cooled through the solvus it becomes energetically favourable for the Na^+ and K^+ ions to be clustered, strains then being localized at cluster surfaces. Lamellar clusters remain coherent and coarsen as described in Sheet 2, Sec. 2 (Note 9). There is no charge coupling between the *M* and *T* ions.

In contrast, in PL the ionic radii of Na^+ and Ca^{2+} are effectively identical, but there is coupling between *M* and *T* ions as each Ca^{2+} ion must be accompanied by an Al^{3+}, replacing Si^{4+} to sustain charge balance. The Si:Al ratio changes from 3:1 in Ab to 1:1 in An. The extreme complexity of chemically intermediate, ordered plagioclase feldspar structures, in which Al and Si are arranged regularly (ordered) on the four equivalent structural sites (see Fig. 1.4), is a result of what is known as Lowenstein's rule, often called Al/Al avoidance. This rule, which applies to many, but not all, framework aluminosilicates, states that whenever two tetrahedra are linked by a common oxygen, only one of them can be occupied by Al. A simple structural diagram is provided by Smith and Brown (1988, fig. 1.1). In *disordered high plagioclase* there are no symmetry-related structural constraints on the position of Si and Al and many ways of distributing Al and Si that do not violate Al/Al avoidance. The solid solution is continuous and close to ideal. However the end-members of the *ordered low plagioclase* series have very different properties because of their different Al:Si ratio. In *low albite* [in which the structure is a slightly distorted version of Fig. 1.4, with all Al in the $T_1(0)$ site (Note 5)] there are no positions in which *additional Al* can be placed (to create a hypothetical oligoclase, for example) that do not violate Al/Al avoidance. On the other hand, it is possible to disorder low albite, by heating, without such violation. In *anorthite*, with its 2:2 Al:Si ratio, there is only one arrangement, in which Al alternates between T_1 and T_2 sites, that does not violate Al/Al avoidance. This arrangement is fully ordered and impossible to disorder. Pure anorthite is always fully ordered except very close to the melting point. However, it is possible to place *additional Si* in the anorthite structure. The two end members of the ordered PL series thus have different ordering schemes.

Together with the coupled exchange of Na ⇌ Ca with Si ⇌ Al, this simple difference in behaviour underlies much of the complexity of low PL, including the three established miscibility gaps and the *e*-plagioclase structure. This structure was recognized in single-crystal diffraction patterns as additional diffraction spots (*e* diffractions) lying symmetrically about *b* diffractions, which have $(h + k)$ odd, l odd. There is one pair in e_1 plagioclase (see fields on Fig. 1.7) and a second, weaker pair in e_2. The presence of such satellite diffractions shows the existence of a slab-like 'superstructure', in which the slabs are arranged in a sequence that is out-of-step, or 'incommensurate', with the overall lattice, with a repeat distance on the scale of a few nm. Although earlier workers imagined that the slabs necessarily varied compositionally, Carpenter (1994) favours the view that the slabs arise fundamentally because of different ordering patterns, leading to alternations in space group. Possible structural models of *e* plagioclase, some of extreme complexity, are reviewed by Smith and Brown (1988, chap. 5). Carpenter's phase diagram (Fig. 1.7), differs from earlier diagrams because it shows stability fields for the *e* structures, separated by the Bøggild solvus. At very low *T* these fields are shown dying out because of the evidence from metamorphic rocks of complete immiscibility (e.g. Wenk 1979).

Carpenter (1994, fig. 20) suggests Gibbs energy–composition relationships in high- and low-PL. Disordered PL (high-PL) behave as near-ideal solid solutions and their composition–activity relationships can be expressed in terms of simple $\Delta G/X$ curves that merge smoothly at the $C\bar{1}-I\bar{1}$ and $C\bar{1}-C2/m$ phase transitions (Fig. 1.7). This cannot be the case for low-PL which must be strongly non-ideal, probably depending on their cooling and annealing history. The fine scale of the intergrowths in low-PL is a result of the coupling of M and T ions which leads to slow exsolution kinetics and tells us nothing about the non-ideality of the solid solution. The relationship between microstructures in low-PL, geological history and PL thermodynamics is a largely unexplored field.

Feldspars 2: phase behaviour

8. *Ab−Or behaviour diagram*

Figure 2.1 is slightly modified from Brown and Parsons (1989, fig. 8b). It shows coherent *phase behaviour*, not stable *phase equilibria*. The stable

equilibrium strain-free solvus has been inserted from Fig. 1.5. The coherent solvus is an attempt to define a curve for equilibrium Si−Al order. Near its critical T it is based on a disordered coherent solvus obtained experimentally by Sipling and Yund (1976) and on its limbs on an ordered coherent solvus of Yund (1974). The coherent solvus is different to the strain-free solvus because the phases on the coherent solvus share a continuous Si,Al−O framework. The different ionic radii of Na^+ and K^+ (see Sheet 1, Sec. 4) mean that the framework in K-rich regions (for example in the lamellar intergrowth in Fig. 2.2b) is slightly expanded relative to that in Na-rich regions, leading to coherency strain energy which must be added to the G/X curve for the Ab−Or solid solution. Strictly speaking, the total strain energy varies with bulk composition (because this defines the surface area of the coherent interfaces) so each bulk composition will have its own coherent solvus. The compositions of the phases on the coherent solvus are not independent of the amounts of the phases, as they would be in a conventional phase diagram. For bulk compositions inside the solvus, although the two main processes of exsolution and framework ordering are still driving microtextural change, the phase assemblage that is adopted is to a large extent governed by the minimization of coherency strain energy. The fields within the solvus are based on Brown and Parsons (1984*b*, 1988), and the evolution of the microtextures discussed in Sheet 2, Sec. 2 and Note 9.

It is important to note that Fig. 2.1 is for hypothetical, An-free feldspars. In an An-free liquid at very high P_{H_2O}, two feldspars, labelled AF and PL, would crystallize in equilibrium at the intersection of the solidus and solvus, as shown in Fig. 1.6. In a real granitic liquid the AF would crystallize with a small amount of An in solid solution, and PL would crystallize with more An, characteristically as an oligoclase, and the two feldspars would lie on a tie-line on the ternary feldspar solvus (AF−PL on Fig. 2.5). The effect of only 1 mol% An on the ternary feldspar solvus for feldspars with Ab:Or in the range typical of granites ($\sim Ab_{30}Or_{70}-Ab_5Or_{95}$) is very large, 200−300ºC (see Fig. 9 in Parsons *et al*. 2009, but note discussion) so that in projection the curves on Fig. 2.1 will be at considerably higher T. Note also that the AF−PL pair will lie on a join that is not parallel to the Ab−Or join.

Figure 2.1 illustrates the basic principles which control the microtextures in a typical granitic AF shown in Figs 2.2b and 2.3. In plutonic rocks AF will crystallize as an homogeneous sanidine, adopting the tweed microtexture of orthoclase as it cools and orders. At or just below the coherent solvus (point B) it will begin to exsolve an Ab-rich second phase, B′. As T continues to fall the B−B′ pair changes composition down the solvus and the perthitic exsolution textures become coarser. The solidus plagioclase, PL, does not participate in these reactions. The original AF and PL phases behave as closed systems. This will lead to the film perthite characteristic of granites illustrated in Figs 2.2b and 2.3. Initially the Si, Al−O framework will remain fully coherent, but as the textures coarsen and the feldspar framework stiffens, coherency strains increase and dislocations nucleate (expressed by the etch-pits in Fig. 2.2b) to lower strain energy. This is a semi-coherent orthoclase film perthite (see Note 9), in the labelled region of Fig. 2.1. Partial or complete reactions with fluids near C lead to much coarser, microporous irregular intergrowths, the vein perthite in Fig. 2.3. During this process of 'deuteric coarsening' (Sheet 2, Sec. 3) the regular intergrowths lose coherency, and phase compositions move onto the strain-free solvus, indicated by C−C′. Tweed orthoclase is often replaced by microcline. At this point, events depicted by the behaviour diagram (Fig. 2.1) have terminated with a stable equilibrium assemblage (Fig. 1.5). This basic exsolution history is common to many plutonic AF and is developed further in Sheet 2, Sec. 2, Note 9 and Sec. 3, Note 10.

9. Strain-controlled exsolution

Strain-controlled perthitic microtextures in AF occur in crystals, or parts of crystals, that are optically clear and largely non-turbid. They vary in orientation, general shape and coarseness depending on bulk composition and cooling rate. Figure 2.2 is a simplified and modernized version of fig. 9 in Brown and Parsons (1988) and shows intergrowths in slowly cooled (i.e. plutonic) AF, as they appear viewed approximately normal to (001). Viewing direction must be considered carefully when describing exsolution textures. Twins on the Albite law [which have (010) as composition plane] are a good guide, coupled with the perfect (001) and (010) cleavages (Fig. 2.6). The significant change to the 1988 drawing is the addition of misfit dislocations on film lamellae in region 2. Although this region

covers AF from subsolvus granitic rocks, dislocations had rarely been encountered in earlier TEM work (summarized by Brown and Parsons, 1984*b*). Subsequent application of the simple etching technique of Waldron *et al*. (1994) has shown that dislocations are an almost universal feature of film lamellae in plutonic Or-rich feldspars. Dislocations nucleate on the interfaces of exsolution lamellae. Coherency demands that lattice planes bend at the coherent interface because of the different cell dimensions of the two phases. Introducing periodic dislocations lowers the magnitude of the distortion and minimizes strain, although residual strains persist between the dislocations. The paired etch pits in Fig. 2.2b are the outcrops of single, lens-shaped dislocation loops which encircle the albite lamellae.

A strain-controlled perthite like that in Fig. 2.2b (Lee *et al*., 1995) is semicoherent, and the Ab- and Or-rich phases lie on a solvus curve between the coherent and strain-free solvi on Fig. 2.1. The Or-rich feldspar in Fig. 2.2b is tweed orthoclase. Recent TEM work (Fitz Gerald *et al*., 2006) has shown that reactions with geological fluids have often caused dissolution of strained structure around dislocations, leading to networks of tiny 'nanotunnels'. Dislocations are not found in extremely Or-rich bulk compositions (region 1) because the small size of the lenticular lamellae means that coherency strains can be accommodated without nucleation of dislocations. The dislocations are important in a wide range of geological environments, summarized by Parsons and Lee (2005). During weathering, dissolution occurs rapidly along these features leading to rapid mechanical degradation and accelerating dissolution rates by increasing reactive surface area (Lee and Parsons, 1995; Lee *et al*., 1998). During diagenesis of clastic sedimentary rocks, feldspar dissolution, leading to secondary porosity, is strongly sensitive to their presence, leading to what has been called 'microtextural winnowing' (Parsons *et al*., 2005). It has been suggested that tubular honeycombs in weathered feldspars may have provided reactors and a protected environment for the emergence of the first life (Parsons *et al*., 1998).

The orientation of coherent lamellar interfaces corresponds with planes of minimum coherency strain energy and varies with bulk composition (Fig. 2.2). The orientation of these planes was calculated by Willaime and Brown (1974) using elastic stiffness coefficients for the intergrown phases. The simplest intergrowths are fine lenticular cryptoperthite lamellae in regions 1−3, which like the film microperthite lamellae in Figs 2.2b and 2.3 are in an irrational plane (i.e. a plane without integer Miller indices) between $(\bar{6}01)$ and $(\bar{8}01)$. In volcanic rocks, when the lenticular lamellae are thinner and shorter than those in Figs 2.2b and 2.3, misfit dislocations do not develop and it is possible to estimate cooling rates from the wavelength of the exsolution texture. A good review of alkali feldspar exsolution kinetics was provided by Yund (1984). However the relationship used by Yund to relate wavelength λ to annealing time, $\lambda = \lambda_0 + kt^{1/3}$ (where λ_0 is a small initial wavelength, k is a coarsening-rate constant which varies with T, and t is time) is for spherical intergrowths. For planar intergrowths $\lambda^2 = \lambda_0^2 + kt$ is appropriate (Brady, 1987). The relationships give similar coarsening rates for t up to a few years but differ significantly over geological time-scales. An interesting application of the method to the well known Bishop Tuff was provided by Snow and Yund (1988).

With slow cooling the coherent exsolution textures in feldspars in region 2 (Fig. 2.2) continue to coarsen and misfit dislocations develop. The Or-rich phase is often tweed orthoclase. Yuguchi and Nishiyama (2007) showed that the periodicity of coarse intergrowths like those in Figs 2.2b and 2.3 could be related to cooling rate, deduced from heat transfer models in a granite pluton. The observed change in lamellar spacing is in the range 5 to 15 μm.

Microtextures in more albitic AF, in region 4 (Fig. 2.2), are complex and lead to the fully coherent texture known as braid perthite (fig. 2.2a, from Brown *et al*., 1983, and fig. 2.4, from Parsons and Lee, 2009). Braid perthite is common in syenitic rocks in parts of feldspars that have escaped interactions with fluids. The Oslo larvikite, with its iridescent cryptoperthitic AF, is a familiar example. Braid texture consists (Fig. 2.2a) of diamond shaped areas (actually columns) of Albite-twinned low albite defined by zig-zag lamellae of low microcline. Each zig and each zag in the microcline is a twin in the relationship known as the diagonal association, a deformed twin between the positions of Albite and Pericline twinning (Fig. 2.8). The interface of the lamellae is $\{\bar{6}\bar{6}1\}$, referred to the triclinic microcline lattice. The evolution of braid texture was established using TEM by Brown *et al*.

(1983) and Brown and Parsons (1984*a*) in the layered Klokken syenite intrusion in which the microtextures evolve systematically downwards from the roof. Exsolution begins with the formation of straight lamellae which become slightly zig-zag as the Or-rich phase orders to produce intermediate microcline (Note 6c). Most coherent coarsening occurs close to the coherent solvus, because diffusion rates decrease as *T* decreases. Recent modelling of coarsening following spinodal decomposition (see this Section, below) by Abart *et al*. (2009) suggests that most coarsening occurs within 30ºC of the coherent spinodal, which is close to the coherent solvus in these feldspars. As further ordering occurs, the interfaces rotate into the $\{\bar{6}\bar{6}1\}$ orientation of low microcline and zigs and zags coalesce to produce the texture in Fig. 2.2a. In the Klokken intrusion the log of the periodicity, λ, of the Or-rich lamellae increases linearly downwards, from ~30 nm at the top of the layered series to a maximum of ~400 nm at the base of the 600 m section exposed. This suggests that the microtextures have evolved in response to cooling through the roof of the intrusion. However, their fine scale is comparable with that found in volcanic rocks. It is probable that ordering, and the twinning associated with it, slows coarsening because of the need to exchange Al between T_1 sites (Note 5) as coarsening proceeds. Cooling rates cannot be calculated from lamellar periodicities because ordering is too slow for laboratory calibration.

The reason that the Or-rich feldspar in braid perthite is microcline, while in film perthites (Figs 2.2b, 2.3) it is often orthoclase, is not related to cooling rates. The Klokken intrusion is small and cooled through the exsolution and coarsening interval in <10,000 y (Brown and Parsons, 1984*a*, fig. 10) whereas many batholithic granites contain tweed orthoclase. Braid microperthite crystals have bulk compositions close to $Ab_{60}Or_{40}$ (Fig. 2.2). Microcline in the zig-zag diagonal association forms relatively easily because the Or-rich lamellae are intergrown with a volumetrically dominant, Ab-rich phase, which because of the shearing transformation (ST on Fig. 2.1), becomes triclinic early in the coarsening process (see Note 12). Relatively large 'left–right' (often called 'order–antiorder') zig-zag domains develop in the Or-rich phase which coarsen quickly to minimize coherency strain with the dominant Ab-rich phase. It must be stressed that all features of the complex braid microtexture, including compositional lamellar interfaces, relatively short-period Albite twins in albite, and the long-period diagonal twins in microcline, are orientated and spaced to minimize coherency strain energy. Atomic diffusion has occurred down chemical potential gradients dominated by chemically derived elastic strain, which in the case of the Klokken intrusion has persisted for 1.166 Ga.

In the more Or-rich bulk compositions of AF in many granites (~$Ab_{30}Or_{70}$–Ab_5Or_{95}) the Ab-rich phase is subordinate in volume and cannot control, through coherency strain, the development of wavy twins in microcline. Instead the Or-rich phase develops the short-period domain texture of orthoclase, and albite exsolution lamellae remain straight. In region 5 (Fig. 2.2), where the Ab-rich phase is volumetrically dominant but also high in An, migration of lamellar interfaces cannot occur because of the need for Al and Si in the strong framework to diffuse as well as alkali ions. The Or-rich phase is again tweed orthoclase. The contrasting behaviour of the feldspars in Figs 2.2a and b illustrates how, in coherent intergrowths, coherency strains control not only phase compositions but also phase transitions.

Because of space considerations the Posters do not describe the mechanisms by which exsolution begins. Reviews are given by Yund (1984) and the textbook of Putnis (1992, chapter 8) contains an excellent account. There are two fundamental mechanisms. Which occurs depends on bulk composition, initial *T* of crystal growth and cooling rate. In compositions fairly close to the critical *T* of the ternary solvus (regions 3–5, Fig. 2.2) the most likely mechanism is known as spinodal decomposition. During spinodal unmixing, a low-amplitude compositional modulation develops, by clustering of Na^+ and K^+ ions. The texture looks similar, in TEM images, to the tweed texture in orthoclase (Fig. 2.9) and initially has a single lattice. The amplitude of the modulation rapidly increases and discrete Ab- and Or-rich lamellae (two lattices) develop with a distinct initial periodicity λ_0. With time this periodicity increases according to the rate laws given above. Spinodal decomposition begins at a coherent spinodal curve which lies inside the coherent solvus and touches it at the critical *T*. A rapidly cooled feldspar may pass through the coherent solvus uneventfully, but unless it is cooled extremely quickly it will always unmix at the coherent spinodal. Owen and McConnell

(1974) showed experimentally that an AF of composition $Ab_{63}Or_{37}$ underwent spinodal decomposition in <1 h when annealed between 500 and 600ºC, a very rapid geological process.

AF with bulk compositions on the flanks of the solvus are unlikely to unmix by a spinodal mechanism, because they will not intersect the spinodal curve until they reach low *T*. When cooling under plutonic conditions they can potentially begin to unmix just below the coherent solvus (at B on Fig. 2.1). Unmixing begins by nucleation of the second phase at B′. In this example Na^+ will diffuse from the mixed initial feldspar to an Ab-rich nucleus, depleting the matrix locally in Na. As usual with a nucleation process the nucleus must achieve a critical size to become stable, when the gain in free energy due to the surface is less than the free energy lost by exsolution. Nucleation can be coherent or incoherent, and homogeneous (arising spontaneously in perfect structure) or heterogeneous (nucleation on a pre-existing defect or inclusion). It is probable that textures like that in Fig. 2.2b form by coherent homogeneous nucleation.

Coherent, strain-controlled intergrowths in both AF and PL have important geochemical implications. The crystals retain elastic strains that can develop only following continuous, coherent exsolution, and which are not preserved when dissolution–reprecipitation reactions occur. The periodic intergrowths provide robust markers of the bulk chemical composition (with respect to major elements, trace elements, and isotopes) of the crystals at the time when coherent exsolution began. Possible chemical changes affecting the bulk crystals could occur only in the interval between crystal growth and the beginning of coherent exsolution, except perhaps close to crystal faces when intergrowths would be modified. Because most AF in plutonic rocks are mixtures of strain-controlled and recrystallized microtextures (e.g. Figs 2.3, 2.4), estimates of crystal composition at the time of growth are best obtained from bulk analyses of coherent microtextures than bulk analyses of whole crystals (Note 10).

10. Replacement reactions and deuteric coarsening

Many feldspar crystals are partly or completely turbid in thin section. There is a clear correlation between optical turbidity and marked coarsening of perthite, which loses the regularity of the strain-controlled intergrowths (Parsons, 1978). This correlation can be seen in Fig. 2.3, from Parsons *et al*. (2005, fig. 5). The process was called 'deuteric coarsening' by Parsons and Brown (1984) following terminology introduced by Alling (1932), who recognized correctly that perthites could be formed by both exsolution and replacement processes. Worden *et al*. (1990) showed, using TEM, that turbid regions in feldspars from the Klokken intrusion (Fig. 2.4 right) corresponded with profound recrystallization of the original strain-controlled braid microtexture. The patch perthite is a mosaic of incoherent albite and microcline subgrains on scales from 10s of nm to >100 μm (see e.g. Parsons and Lee, 2009, fig. 6). Its features correspond with all the criteria suggested by Putnis (2002) to be distinctive of *in situ* replacement. The black dots (Fig. 2.4 right) correspond with the micropores which cause turbidity, most of which have formed at the junctions between subgrains which maintain the orientation of the overall original crystal (Walker *et al*., 1995). They are strikingly absent from the pristine braid perthite (Fig. 2.4 left). Brown and Parsons (1993) developed the idea that the reactions are driven by release of coherency strain energy during dissolution–reprecipitation reactions. The reactions in the Klokken feldspars do not involve changes in bulk composition (Brown *et al*., 1983) and Smith and Brown (1988, p. 596) suggested that the process should be called 'mutual replacement'. A detailed treatment of the process has recently been provided by Parsons and Lee (2009) and the partitioning of trace elements between the Ab- and Or-rich patches has been described by Parsons *et al*. (2009). It seems that the replacement reactions take place in thin fluid films that advance as fronts through the braid perthite, converting it to incoherent subgrain mosaics. The reaction front can be sharp (Fig. 2.4) or take place over a few 10s of μm.

Replacement in feldspars is often not isochemical, however. The turbid regions of Fig. 2.3 have been subject to two phases of replacement (Lee and Parsons, 1997). The irregular vein perthite at the top of the image, which cuts obliquely across the semicoherent film lamellae and is microtexturally equivalent to the patch perthite in Fig. 2.4, contains an oligoclase ($\sim Ab_{90}An_9Or_1$) and cannot have formed from the pre-existing film perthite. Replacement must therefore be non-isochemical. The turbidity associated with film lamellae at the bottom of

the image is associated with outgrowths of very pure albite ($Ab_{>99}$) on film lamellae, which have nucleated on the misfit dislocations. The reactant fluid entered the crystals *via* the nanotunnels described by Fitz Gerald *et al*. (2006). In the outer parts of crystals this 'pure replacive albite' spreads in three dimensions to produce irregular regions >100 μm across occupying ~25% by volume of the original grain, considerably larger than the volume of albite in unaltered crystals (Fig. 2.2b). Again, replacement in this case cannot have been isochemical.

Replacement of clastic feldspars by albite during diagenesis ('albitization') is a well established phenomenon (e.g. Milliken, 1989; many other examples are given by Parsons *et al*. 2005). As well as the example above, albitization in igneous rocks has been reported by a number of authors although not often with microtextural detail. Envik *et al*. (2008) describe in detail the replacement of original oligoclase by pure albite in a tonalite. Replacement of albite by microcline has been found in AF phenocrysts from the Shap granite incorporated in a conglomerate that overlies the intrusion. Albite lamellae in orthoclase (Fig. 2.2b) are replaced piecemeal by microcline, retaining the original lamellar texture (Lee and Parsons, 1998). The same relationship can occasionally be observed in feldspars collected from the igneous rock, but it is not widespread. Putnis *et al*. (2007) describe extensive replacement of plagioclase by K-feldspar. Putnis (2009) has provided a comprehensive review of replacement reactions in general. It is indeed surprising, as Putnis *et al*. point out, that the mineralogical evidence for subsolidus re-equilibration in granitic rocks is largely ignored in geochemical studies.

II. Ternary equilibria and geothermometry

Figure 2.5 is a simplified version of fig. 1 in Parsons *et al*. (2005) and is intended to show general features only. The purple surface SFS represents the strain-free ternary solvus and the blue surface CS represents the coherent ternary solvus. The two surfaces are assumed to be parallel. The horizontal surface is an isotherm on the dome-shaped strain-free solvus which in an igneous rock would represent the solidus–solvus intersection, on which two feldspars, PL and AF, would crystallize on a tie-line. Because the solvus depicts reactions involving feldspar phases and components only, its shape depends solely on T and P and not on the bulk composition of the host rock. The solidus T, on the other hand, depends on magma composition and particularly strongly on P_{H_2O} (Note 6a). The tie-lines between AF and PL feldspar pairs depend on T and less strongly on P, and, provided some estimate of P can be made, the compositions of feldspar pairs provide a geothermometer applicable to both igneous and metamorphic rocks. The most striking feature of the ternary solvus surface is its extreme sensitivity to small concentrations of An in AF and Or in PL. The definitive paper on two-feldspar–liquid phase relationships is Brown (1993).

Early attempts to construct two-feldspar geothermometers treated AF and PL as independent binary solid solutions, but the thermodynamic principles behind a thermometer for two ternary solid solutions were given by Brown and Parsons (1981). The basic principle is that the chemical potential, μ, of each component must be the same in both phases: $\mu_{Or}^{AF} = \mu_{Or}^{PL}$, $\mu_{Ab}^{AF} = \mu_{Ab}^{PL}$, $\mu_{An}^{AF} = \mu_{An}^{PL}$. A number of computerized versions are available based on thermodynamic mixing models of the two ternary solutions, of which the most widely used are Fuhrman and Lindsley (1988) and Elkins and Grove (1990). They are based partly on limited volumetric and calorimetric thermodynamic data and partly on a phase equilibrium study of ternary feldspars by Seck (1971), although Johannes (1979) and Brown and Parsons (1981, 1985) expressed doubt that these experiments represented equilibrium, a position confirmed by later experiments by Elkins and Grove (1990). The thermometers may be accessed on line by using the package SOLVCALC (Wen and Nekvasil, 1994). A modified thermometer, which gives better agreement with naturally occurring assemblages, has recently been developed, using calorimetric data, by Benisek *et al*. (2010).

All the present thermometers are based on feldspars with Si–Al disorder and are unlikely to work well below ~700ºC. It is possible to estimate the effects of order by making corrections based on the ordered solvus curves of Bachinski and Müller (1971) and Müller (1971) but these are binary solvi and the form of an ordered ternary solvus surface is not known. In a similar way it is possible to make rough estimates of the position of ternary coherent solvi based on the position of the binary coherent solvi of Sipling and Yund (1976) for disordered feldspars and of Yund (1984) for ordered feldspars. A recent example of an attempt to obtain two-feldspar T in ordered

feldspars is Parsons *et al*. (2009). The extremely large effect of An on the ternary solvus for Or-rich feldspars (1 mol% An raises the solvus by ~300ºC for $Ab_{90}Or_{10}$, their fig. 9) is likely to remain problematical for the study of low-*T* fluid–feldspar reactions.

12. Twinning and phase transitions

Smith and Brown (1988, chapter 18) describe the twin laws in feldspars, their structural basis, and their genesis. There are about 20 twin laws but only five are common. The large number of twin laws is a consequence of the high pseudosymmetry of the feldspar structure. For example, an individual Albite twin in PL is close to monoclinic in symmetry, and a pair of Albite twins has overall monoclinic symmetry. Simple Carlsbad, Baveno and Manebach twins can occur in all feldspars and develop during growth. Repeated 'polysynthetic' twinning can occur only in triclinic feldspars but is extremely common. The polysynthetic twin laws are the Albite law [twin plane (010), twin axis (010), composition plane (010)] and the Pericline law [twin plane an irrational plane (see Note 9 for a definition) perpendicular to *b*, twin axis *b*, composition plane an irrational plane {*h*0*l*} called the rhombic section, see next paragraph]. Polysynthetic twins can form during growth, in response to applied stresses, and as a result of changes in symmetry. Symmetrical extinction angles of Albite twins, and combined Carlsbad–Albite twins, provide routine methods for obtaining the composition of plagioclase, covered in most mineralogy text books.

It is useful to understand the relationship between exsolution features, polysynthetic twins and cleavages. For SEM and TEM work it is helpful to polish or to thin samples in known orientations, and cleavage fragments, which are commonly defined by (001) and (010) cleavages, are a good starting point. Figure 2.6 shows a perthitic alkali feldspar cleavage fragment lying on its (010) cleavage, so that Albite twins are parallel to the page. All angles are accurate. Such fragments are often defined by the (001) cleavage and the 'Murchison plane', a plane of easy fracture which is an irrational plane between $(\bar{6}01)$ and $(\bar{8}01)$. In plutonic AF this plane is probably defined by the rows of misfit dislocations, usually converted to nanotunnels (Fitz Gerald *et al*., 2006), on the surface of film albite exsolution lamellae, shown in orange. The lenticular shape of these lamellae is exaggerated; in reality they are nearly straight (Fig. 2.2b). The misfit dislocation loops are joined, across albite lamellae, by minute cleavage cracks, parallel to (001), called 'pull-aparts' by Fitz Gerald *et al*. Pericline twins are at right angles to (010), but their composition plane, the so-called 'rhombic section', rotates about *b* depending on composition and framework order. The geometry of the rhombic (better called 'rectangular') section is shown by Smith and Brown (1988, fig. 18.3). Its position is strongly sensitive to small changes in the cell angles. The position of Pericline twins in Fig. 2.6 is taken from fig. 18.8 in Smith and Brown (1988). In microcline they are almost at right angles to (001) and when the cross-hatched 'tartan' twinning is visible in a thin section, only a single cleavage, (010), is visible (Fig. 2.8). In high albite and anorthoclase, Pericline twins are almost parallel to (001). When cross-hatched twinning is visible in anorthoclase both (010) and (001) cleavages are visible (Fig. 2.7). In low albite, Pericline twins are almost normal to *Z*, but in calcic plagioclase (not shown) the rhombic section rotates progressively anticlockwise past the *X* axis, eventually making an angle of 18º with *X* in anorthite. Once a Pericline twin has formed, it does not change position with subsequent ordering. Thus Fitz Gerald *et al*. (2006) found that Pericline twins in the Shap feldspars were in the high albite position, although they are now ordered low albite.

13. Twinning in anorthoclase and perthitic albite

Combined Albite and Pericline twins in anorthoclase and microcline form in response to monoclinic–triclinic phase transitions but the mechanisms are different. In anorthoclase the twins form at the shearing transformation (ST in Figs. 1.5 and 2.1). In principle the spontaneous shearing of the framework could be in the same sense over long distances but in practice crystals are normally constrained in some way that favours preservation of the original monoclinic *C*2/*m* symmetry, which is maintained by the overall twinned crystal. If the crystal in Fig. 2.7 were viewed in a microscope with a high-*T* stage, the birefringence contrast between adjacent lamellae would decrease as the crystal was heated towards ST, vanishing completely at the transition. On cooling through ST the twins would reappear. The twinning in anorthoclase is

generally more sharply defined than in microcline (compare with Figs 2.8 and 2.9) and twins have parallel sides rather than spindle shapes. Some microcline can have regular twins, however, and the orientation relative to cleavages is then diagnostic.

Albite twinning in coherent albite exsolution lamellae also forms at the shearing transformation, when the Ab-rich phase encounters the intersection of ST with the coherent solvus (Fig. 2.1). Initially the twins have long periodicity (Brown and Parsons, 1984*a*) which decreases on cooling. The periodicity of the twins (e.g. those in Fig. 2.2a) depends on the thickness of the exsolution lamella, and on the departure of the α and γ angles of each twin from 90º (Willaime and Gandais, 1972). If lamellae continue to coarsen after twinning the twin periodicity would be expected to adjust itself to local lamellar thickness (McLaren, 1974; see Brady, 1987 for a description of the coherent coarsening process). However, as Fig. 2.2a shows, the twins in braid perthite are of constant thickness even though the diamond-shaped braid areas taper markedly. Brown and Parsons (1984*a*) suggested that primary lamellar coarsening did not continue after twins had formed, and textural changes were restricted to rotation of the albite–microcline interfaces into $(\bar{6}\bar{6}1)$ (Note 9). This is consistent with the slowing of diffusion with falling *T* and the modelling of Abart *et al*. (2009).

14. Twinning in microcline

Intersecting Albite and Pericline twins in microcline ('tartan' twinning) form as a consequence of convergent ordering by diffusion of Al onto the $T_1$0 site (see Note 5). The twins are often diffuse, of variable thickness and spindle-shaped in projection (Fig. 2.8), although more regularly twinned microcline is known. TEM shows that regions of orthoclase, with tweed texture, are often present in microcline crystals [e.g. fig. 2.9, from Fitz Gerald and McLaren (1982)]. There is general agreement that tweed orthoclase formation (Note 5) usually precedes microcline formation and there is evidence of a progressive development *via* irregular microcline to regularly twinned crystals (Bambauer *et al*., 1989). However, the mechanism of the steps from tweed to tartan is not clear (Note 5). Unlike twins in anorthoclase, twins in microcline, and tweed texture in orthoclase, survive heating for long periods near the solidus, because Si−Al disordering is relatively slow even at high *T* (Parsons *et al*., 2010).

Not all microcline has tartan twinning. The low-*T* variety of K-feldspar, adularia, which is characterized by a distinctive {110} habit, can be highly ordered but untwinned, or can be highly disordered. This suggests that untwinned microcline may grow directly as a triclinic phase at low *T*, the degree of order perhaps depending on growth rate. Authigenic microcline growing in the 250−360ºC interval in the Salton Sea geothermal system (McDowell, 1986) has both Albite and Pericline twins. These do not intersect but form in different regions of the crystal, with blunt terminations against the other twin type. An unusual style of tiled twinning in microcline from a nepheline-eudialyte syenite from the Ilímaussaq intrusion (Smith and McLaren, 1983) may indicate growth in the microcline stability field. These rocks have very low solidus *T*, perhaps as low as 500ºC. There is, therefore, evidence that under some conditions microcline can form without a monoclinic precursor.

15. Twinning in plagioclase

Twinning in plagioclase is reviewed in detail by Smith and Brown (1988, chapter 18). Polysynthetic *growth twins* can be recognized by the following features: (1) They are usually of low to moderate frequency in a given crystal. (2) They often have stepped composition surfaces and may stop abruptly. (3) They may thicken or thin independently of each other. *Glide twins*, produced by deformation: (1) occur in weakly or strongly deformed crystals; (2) are often lenticular or taper to a point; (3) may occur in clusters that vary in thickness sympathetically; or (4) are related to internal features such as cleavages, cracks or kinks, or to the grain boundary. It is relatively easy to produce glide twins in deformation apparatus in ordered plagioclase for compositions with >20% An, but it is difficult to form glide twins in more albitic crystals. The initial products of deformation may strictly be pseudotwins, because the sites occupied by Si and Al are incorrect in the deformed structure. Pseudotwins may turn into true twins by diffusion over time. Intersecting Albite and Pericline twins may develop by glide in the 'M' relationship characteristic of microcline (see Smith and Brown, fig. 18.18).

References

Abart, R., Petrisheva, E., Wirth, R. and Rhede, D. (2009) Exsolution by spinodal decomposition II: Perthite formation during slow cooling of anatexites from Ngoronghoro, Tanzania. *American Journal of Science*, **309**, 450–475.

Alling, H.L. (1932) Perthites. *American Mineralogist*, **17**, 43–65.

Bachinski, S.W. and Müller, G. (1971) Experimental determination of the microcline–low albite solvus. *Journal of Petrology*, **12**, 329–356.

Bambauer, H.U., Krause, C. and Kroll, H. (1989) TEM investigation of the sanidine/microcline transition across metamorphic zones. *European Journal of Mineralogy*, **1**, 47–58.

Benisek, A., Dachs, E. and Kroll, H. (2010) A ternary feldspar mixing model based on calorimetric data: development and application. *Contributions to Mineralogy and Petrology*, DOI: 10.1007/s00410-009-0480-8.

Bowen, N.L. (1913). The melting phenomena of the plagioclase feldspars. *American Journal of Science*, **35**, 577–599.

Brady, J.B. (1987) Coarsening of fine-scale exsolution lamellae. *American Mineralogist*, **72**, 697–706.

Brown, W.L. (1993) Fractional crystallization and zoning in igneous feldspars: ideal water-buffered liquid fractionation lines and feldspar zoning paths. *Contributions to Mineralogy and Petrology*, **113**, 115–125.

Brown, W.L. editor (1984) *Feldspars and Feldspathoids. Structures, Properties and Occurrences*. NATO ASI Series C 137. D. Reidel Publishing Company, Dordrecht, The Netherlands 541 pp.

Brown, W.L. and Parsons, I. (1981) Towards a more practical two feldspar geothermometer. *Contributions to Mineralogy and Petrology*, **76**, 369–377.

Brown, W.L. and Parsons, I. (1984*a*) Exsolution and coarsening mechanisms and kinetics in an ordered cryptoperthite series. *Contributions to Mineralogy and Petrology*, **86**, 3–18.

Brown, W.L. and Parsons, I. (1984*b*) The nature of potassium feldspar, exsolution microtextures and development of dislocations as a function of composition in perthitic alkali feldspars. *Contributions to Mineralogy and Petrology*, **86**, 335–341.

Brown, W.L. and Parsons, I. (1985) Calorimetric and phase-diagram approaches to two-feldspar geothermometry: a critique. *American Mineralogist*, **70**, 356–361

Brown, W.L. and Parsons, I. (1988) Zoned ternary feldspars in the Klokken intrusion: exsolution textures and mechanisms. *Contributions to Mineralogy and Petrology*, **98**, 444–454.

Brown, W.L. and Parsons, I. (1989) Alkali feldspars: ordering rates, phase transformations and behaviour diagrams for igneous rocks. *Mineralogical Magazine*, **53**, 25–42.

Brown, W.L. and Parsons, I. (1993) Storage and release of elastic strain energy: the driving force for low temperature reactivity and alteration of alkali feldspars. Pp. 267–290 in: *Defects and Processes in the Solid State: Geoscience Applications. The McLaren Volume.* (J.N. Boland, and J.D. Fitz Gerald, editors). Elsevier Science Publishers B.V, Amsterdam.

Brown, W.L., Becker, S.M. and Parsons, I. (1983) Cryptoperthites and cooling rate in a layered syenite pluton. *Contributions to Mineralogy and Petrology*, **82**, 13–25.

Buntebarth, G. (1991) Thermal models of cooling. Pp. 379–402 in: *Equilbrium and Kinetics in Contact Metamorphism.* (G. Voll, J. Töpel, D.R.M. Pattison and F. Seifert, editors). Springer-Verlag, Berlin.

Carpenter, M.A. (1994) Subsolidus phase relations of the plagioclase feldspar solid solution. Pp. 221–269 in: *Feldspars and their Reactions* (I. Parsons, editor). NATO ASI Series C 421. Kluwer Academic Publishers, Dordrecht, The Netherlands.

Carpenter, M.A and Salje, E.K.H. (1994) Thermodynamics of nonconvergent cation ordering in minerals. *American Mineralogist*, **79**, 1084–1098.

Christie, O.H.J. editor (1962) *Feldspar Volume. Bind 42.2 Halvbind.* Norsk Geologisk Tidsskrift, Norsk Geologisk Forening, Oslo, 606 pp.

Deer, W.A., Howie, R.A and Zussman, J. (2001) *Rock-Forming Minerals, Volume 4A, Framework Silicates: Feldspars*. The Geological Society, London, viii + 972 pp.

Eggleton, R.A. and Buseck, P.R. (1980) The orthoclase-microcline inversion: a high resolution transmission electron microscope study and strain analysis. *Contributions to Mineralogy and Petrology*, **74**, 123–133.

Elkins, L.T. and Grove T.L. (1990) Ternary feldspar experiments and thermodynamic models. *American Mineralogist*, **75**, 544–559.

Envik, A.K., Putnis, A., Fitz Gerald, J.D. and Austrheim, H. (2008) Albitization of granitic rocks: the mechanism of replacement of oligoclase by albite. *The Canadian Mineralogist*, **46**, 1401–1415.

Fitz Gerald, J.D. and McLaren, A.C. (1982) The microstructures of microcline from some granitic rocks and pegmatites. *Contributions to Mineralogy and Petrology*, **80**, 219–229.

Fitz Gerald, J.D., Parsons, I. and Cayzer, N. (2006) Nanotunnels and pull-aparts: Defects of exsolution lamellae in alkali feldspars. *American Mineralogist*, **91**, 772–783.

Flehmig, W. (1977) The synthesis of feldspars at temperatures between 0º–80ºC, their ordering behaviour and twinning. *Contributions to Mineralogy and Petrology*, **65**, 1–9.

Folk, R.L. (1955) Note on the significance of turbid feldspars. *American Mineralogist*, **40**, 356–357.

Fuhrman, M.L. and Lindsley, D.L. (1988) Ternary feldspar modelling and thermometry. *American Mineralogist*, **73**, 201–215.

Goldsmith, J.R. and Jenkins, D.M. (1985) The high–low albite relations revealed by reversal of degree of order at high pressure. *American Mineralogist*, **70**, 911–923.

Harker, R.I. (1954) The occurrence of orthoclase and microcline in the granitic gneisses of the Carn Chuinneag-Inchbae complex, E. Ross-shire. *Geological Magazine*, **91**, 129–136.

Harker, R.I. (1962) The older orthogneisses of Carn Chuinneag and Inchbae. *Journal of Petrology*, **3**, 215–237.

Henderson, C.M.B. (1984) Feldspathoid stabilities and phase inversions – a review. Pp. 471–499 in: *Feldspars and Feldspathoids. Structures, Properties and Occurrences.* (W.L. Brown, editor). NATO ASI Series C 137. D. Reidel Publishing Company, Dordrecht, The Netherlands.

Hofmeister, A.M. and Rossman, G.R. (1983) Color in feldspars. Pp. 271–280 in: *Feldspar Mineralogy* (P.H. Ribbe, editor). Mineralogical Society of America, Washington, D.C.

Hovis, G.L., Delbove, F. and Roll Bose, M. (1991) Gibbs energies and entropies of K-Na mixing for alkali feldspars from phase equilibrium data: Implications for feldspar solvi and short-range order. *American Mineralogist*, **76**, 913–927.

Johannes, W. (1979) Ternary feldspars: kinetics and possible equilibria at 800ºC. *Contributions to Mineralogy and Petrology*, **68**, 221–230.

Johannes, W. (1994) Partial melting reactions of plagioclase and plagioclase-bearing systems. Pp. 161–194 in: *Feldspars and their Reactions* (I. Parsons, editor). NATO ASI Series C 421. Kluwer Academic Publishers, Dordrecht, The Netherlands.

Johnson, E.A. and Rossman, G.R. (2004) A survey of hydrous species and concentrations in igneous feldspars. *American Mineralogist*, **89**, 586–600.

Kroll, H. and Bambauer, H.-U. (1981) Diffusive and displacive transformation in plagioclase and ternary feldspar series. *American Mineralogist*, **66**, 763–769.

Kroll, H. and Knitter, R. (1991) Al,Si exchange kinetics in sanidine and anorthoclase and modeling of rock cooling paths. *American Mineralogist*, **76**, 928–941.

Kroll, H., Bambauer, H.-U. and Schirmer, U. (1980) The high albite–monalbite and analbite–monalbite transitions. *American Mineralogist*, **65**, 763–769.

Kroll, H., Krause, C. and Voll, G. (1991) Disordering, re-ordering and unmixing in alkali feldspars from contact-metamorphosed quartzites. Pp. 267–296 in: *Equilibrium and Kinetics in Contact Metamorphism* (G. Voll, J. Töpel, D.R.M. Pattison and F. Seifert, editors). Springer-Verlag, Berlin.

Laves, F. (1950) The lattice and twinning of microcline and other potash feldspars. *Journal of Geology*, **58**, 548–547.

Laves, F. (1960) The feldspars: their polysynthetic twinning and their phase relations. *Rendiconti della Societá Italiana di Mineralogia e Petrologia*, **16**, 37–100.

Lee, M.R. and Parsons, I. (1995) Microtextural controls of weathering of perthitic alkali feldspars. *Geochimica Cosmochimica Acta*, **59**, 4465–4488.

Lee, M.R. and Parsons, I. (1997) Dislocation formation and albitization in alkali feldspars from the Shap granite. *American Mineralogist*, **82**, 557–570.

Lee, M.R. and Parsons, I. (1998) Microtextural controls of diagenetic alteration of detrital alkali feldspars: a case study of the Shap conglomerate (Lower Carboniferous), Northwest England. *Journal of Sedimentary Research*, **68**, 198–211.

Lee, M.R., Waldron, K.A., Parsons, I. (1995) Exsolution and alteration microtextures in alkali feldspar phenocrysts from the Shap granite. *Mineralogical Magazine*, **59**, 63–78.

Lee, M.R., Hodson, M.E. and Parsons, I. (1998) The role of intragranular microtextures and microstructures in chemical and mechanical weathering: direct comparisons of experimentally and naturally weathered alkali feldspars. *Geochimica et Cosmochimica Acta*, **62**, 2771–2788.

Mackenzie, W.S. (1952) The effect of temperature on the symmetry of high temperature soda-rich feldspars. *American Journal of Science*, *Bowen volume*, 319–342.

Mackenzie, W.S. (1957) The crystalline modifications of $NaAlSi_3O_8$. *American Journal of Science*, **255**, 481–516.

MacKenzie, W.S. and Zussman, J. editors (1974) *The Feldspars.* Manchester University Press, UK, xi + 717 pp.

McDowell, S.D. (1986) Composition and structural state of coexisting feldspars, Salton Sea geothermal field. *Mineralogical Magazine*, **50**, 75–84.

McLaren, A.C. (1974) Transmission electron microscopy of the feldspars. Pp. 378–423 in: *The Feldspars* (W.S. MacKenzie, and J. Zussman, editors). Manchester University Press, UK.

Martin, R.F. (1969) The hydrothermal synthesis of low albite. *Contributions to Mineralogy and Petrology*, **23**, 323–339.

Milliken, K.L. (1989) Petrography and composition of authigenic feldspars, Oligocene Frio Formation,

South Texas. *Journal of Sedimentary Petrology*, **59**, 361–374.

Montgomery, C.W. and Brace W.F. (1975) Micropores in plagioclase. *Contributions to Mineralogy and Petrology*, **52**, 17–28.

Morse, S.A. (1970) Alkali feldspars with water at 5 kb pressure. *Journal of Petrology*, **11**, 221–251.

Müller, G. (1971) Der Einfluss der Al,Si-Verteilung auf die Mischungslücke der Alkali feldspäte. *Contributions to Mineralogy and Petrology*, **34**, 73–79

Owen, D.C. and McConnell, J.D.C. (1974) Spinodal unmixing in an alkali feldspar. Pp. 424–439 in: *The Feldspars* (W.S. MacKenzie, and J. Zussman, editors). Manchester University Press, UK.

Parsons, I. (1978) Feldspars and fluids in cooling plutons. *Mineralogical Magazine*, **42**, 1–17.

Parsons, I., editor (1994) *Feldspars and their Reactions*. NATO ASI Series C 421. Kluwer Academic Publishers, Dordrect, The Netherlands, xxx + 650 pp.

Parsons, I. and Boyd, R. (1971) Distribution of potassium feldspar polymorphs in intrusive sequences. *Mineralogical Magazine*, **38**, 295–311.

Parsons, I. and Brown, W.L. (1984) Feldspars and the thermal history of igneous rocks. Pp. 317–371 in: *Feldspars and Feldspathoids. Structures, Properties and Occurrences* (W.L. Brown, editor). NATO ASI Series C 137. D. Reidel Publishing Company, Dordrecht, The Netherlands.

Parsons, I. and Lee, M.R. (2005) Minerals are not just chemical compounds. *The Canadian Mineralogist*, **43**, 1959–1992.

Parsons, I. and Lee, M.R. (2009) Mutual replacement reactions in alkali feldspars I: microtexures and mechanisms. *Contributions to Mineralogy and Petrology*, **157**, 641–661.

Parsons, I., Lee, M.R. and Smith, J.V. (1998) Biochemical evolution: II. Origin of life in tubular microstructures on weathered feldspar surfaces. *Proceedings of the National Academy of Sciences USA*, **95**, 15173–15176.

Parsons, I., Thompson, P., Lee, M.R. and Cayzer, N. (2005) Alkali feldspar microtextures as provenance indicators in siliciclastic rocks and their role in feldspar dissolution during transport and diagenesis. *Journal of Sedimentary Research*, **75**, 921–942.

Parsons, I., Magee, C.W., Allen, C.M., Shelley, J.M.G. and Lee, M.R. (2009) Mutual replacement reactions in alkali feldspars II: trace element partitioning and geothermometry. *Contributions to Mineralogy and Petrology*, **157**, 663–687.

Parsons, I., Fitz Gerald, J.D., Lee, J.K.W., Ivanic, T. and Golla-Schindler, U. (2010) Time–temperature evolution of microtextures and contained fluids in a plutonic alkali feldspar during heating. *Contributions to Mineralogy and Petrology*, **160**, 155–180.

Putnis, A. (1992) *Introduction to Mineral Sciences*. Cambridge University Press, UK, 457 pp.

Putnis, A. (2002) Mineral replacement reactions: from macroscopic observations to microscopic mechanisms. *Mineralogical Magazine*, **66**, 689–708.

Putnis, A. (2009) Mineral replacement reactions. Pp. 87–124 in: *Thermodynamics and Kinetics of Water-Rock Reaction* (E.H. Oelkers and J. Schott, editors). Reviews in Mineralogy and Geochemistry, **70**. Mineralogical Society of America, Chantilly, Virginia and the Geochemical Society, St. Louis, Missouri, USA.

Putnis, A. and Salje, E. (1992) Tweed microstructures: experimental observations and some theoretical models. *Phase Transitions*, **48**, 85–105.

Putnis, A., Hinrichs, R., Putnis, C.V., Golla-Schindler, U. and Collins, L.G. (2007) Hematite in porous red-clouded feldspars: Evidence of large-scale crustal fluid–rock interaction. *Lithos*, **95**, 10–18.

Ribbe, P.H. editor (1983) *Feldspar Mineralogy*. Reviews in Mineralogy, **2**. Mineralogical Society of America, Washington, D.C.

Ribbe, P.H. (1983) Chemistry, structure and nomenclature of feldspars. Pp. 1–19 in: *Feldspar Mineralogy* (P.H. Ribbe, editor). Reviews in Mineralogy **2**. Mineralogical Society of America, Washington, D.C.

Schairer, J.F. (1950) The alkali-feldspar join in the system $NaAlSiO_4$–$KAlSiO_4$–SiO_2. *Journal of Geology*, **58**, 512–517.

Seck, H. (1971) Koexistierende Alkalifeldspäte und Plagioklase im system $NaAlSi_3O_8$–$KAlSi_3O_8$–$CaAl_2Si_2O_8$–H_2O bei Temperaturen von 650ºC bis 900ºC. *Neues Jahrbuch für Mineralogie, Abhandlungen*, **115**, 315–345.

Sipling, P.J. and Yund, R.A. (1976) Experimental determination of the coherent solvus for sanidine-high albite. *American Mineralogist*, **61**, 897-906.

Smith, J.V. (1974a) *Feldspar Minerals vol. 1, Crystal Structure and Physical Properties*. Springer-Verlag, Berlin, xix + 627 pp.

Smith, J.V. (1974b) *Feldspar Minerals vol. 2, Chemical and Textural Properties*. Springer-Verlag, Berlin, xii + 690 pp.

Smith, J.V. and Brown, W.L. (1988) *Feldspar Minerals vol. 1, Crystal Structure, Physical, Chemical and Microtextural Properties (Second Revised and Extended Edition)*. Springer-Verlag, Berlin, xvii + 828 pp.

Smith, K.L. and McLaren, A.C. (1983) TEM investigation of a microcline from a nepheline syenite. *Physics and Chemistry of Minerals*, **10**, 69–76.

Smith, P. and Parsons, I. (1974) The alkali-feldspar solvus at 1 kilobar water vapour pressure. *Mineralogical Magazine*, **39**, 747–767.

Snow, E. and Yund, R.A. (1988) Origin of cryptoperthites in the Bishop Tuff and their bearing on its

thermal history. *Journal of Geophysical Research*, **93**, 8975–8984.

Su, S.-C., Ribbe, P.H. and Bloss, F.D. (1986) Alkali feldspars: structural state determined from composition and optic axial angle 2*V*. *American Mineralogist*, **71**, 1285–1296.

Taroev, V., Göttlicher, J., Kroll, H., Kashaev, A., Suvarova, L., Pentinghaus H., Bernotat-Wulff, H., Breit, U., Tauson, V. and Lashkevich, V. (2008) Synthesis and structural state of K-feldspars in the system $K[AlSi_3O_8]$–$K[FeSi_3O_8]$. *European Journal of Mineralogy*, **20**, 635–651.

Taylor, W.H. (1933) The structure of sanidine and other feldspars. *Zeitschrift für Kristallographie*, **85**, 425–442.

Waldron, K.A., Parsons, I. and Brown, W.L. (1993) Solution-redeposition and the orthoclase-microcline transformation: evidence from granulites and relevance to ^{18}O exchange. *Mineralogical Magazine*, **57**, 687–695.

Waldron, K.A., Lee, M.R. and Parsons, I. (1994) The microstructure of perthitic alkali feldspars revealed by hydrofluoric acid etching. *Contributions to Mineralogy and Petrology*, **116**, 360–364.

Walker, F.D.L., Lee, M.R. and Parsons, I. (1995) Micropores and micropermeable texture in alkali feldspars: geochemical and geophysical implications. *Mineralogical Magazine*, **59**, 507–536.

Wen, S.X. and Nekvasil, H. (1994) Solvcalc – an interactive graphics program package for calculating the ternary feldspar solvus and for 2-feldspar geothermometry. *Computers and Geosciences*, **20**, 1025–1040.

Wenk, H.-R. (1979) An albite–anorthite assemblage in low-grade amphibolite facies rocks. *American Mineralogist*, **64**, 1294–1299.

Willaime, C. and Gandais, M. (1972) Study of exsolution in alkali feldspars. Calculation of elastic stresses inducing periodic twins. *Physica Status Solidi A*, **9**, 529–539.

Willaime, C. and Brown, W.L. (1974) A coherent elastic model for the determination of the orientation of exsolution boundaries: application to the feldspars. *Acta Crystallographica A*, **30**, 313–331.

Worden, R.H., Walker, F.D.L., Parsons, I. and Brown, W.L. (1990) Development of microporosity, diffusion channels and deuteric coarsening in perthitic alkali feldspars. *Contributions to Mineralogy and Petrology*, **104**, 507–515.

Yoder, H.S., Stewart, D.B. and Smith, J.R. (1957) Feldspars. *Carnegie Institution Washington Yearbook*, **56**, 206–214.

Yuguchi, T. and Nishiyama, T. (2007) Cooling process of a granitic body deduced from the extents of exsolution and deuteric sub-solidus reaction: Case study of the Okueyama granitic body, Kyushu, Japan. *Lithos*, **97**, 395–421.

Yund, R.A. (1974) Coherent exsolution in the alkali feldspars. Pp. 173–183 in: *Geochemical Transport and Kinetics* (A.W. Hoffmann, B.J. Gilletti, H.S. Yoder, Jr. and R.A. Yund, editors). Carnegie Institution of Washington publication **634**.

Yund, R.A. (1984) Alkali feldspar exsolution: kinetics and dependence on alkali interdiffusion. Pp. 281–315 in: *Feldspars and Feldspathoids. Structures, Properties and Occurrences* (W.L. Brown, editor). NATO ASI Series C 137. D. Reidel Publishing Company, Dordrecht, The Netherlands.